Experimental investigation of large-ion-lithophile-element-,high-field-strength-element- and rare-earth-element-partitioning between calcic amphibole and basaltic melt: The effects...

Article *in* Contributions to Mineralogy and Petrology · January 2000

DOI: 10.1007/s004100000181

CITATIONS
100

READS
187

2 authors, including:

D. R. Baker
McGill University
161 PUBLICATIONS **5,197** CITATIONS

SEE PROFILE

Contrib Mineral Petrol (2000) 140: 233–250

Claude Dalpé · Don R. Baker

Experimental investigation of large-ion-lithophile-element-, high-field-strength-element- and rare-earth-element-partitioning between calcic amphibole and basaltic melt: the effects of pressure and oxygen fugacity

Received: 7 August 1998 / Accepted: 7 June 2000

Abstract The effects of pressure and oxygen fugacity (fO_2) on trace element partitioning between pargasitic amphibole and alkali-basaltic melts have been determined at pressures from 1.5 to 2.5 GPa and oxygen fugacities at 2 log units above and below the nickel–nickel oxide buffer. Amphibole crystallization experiments were performed in a piston cylinder apparatus and partition coefficients between amphibole and quenched melt of large-ion-lithophile elements (LILE: Rb, Sr, Ba), high-field-strength elements (HFSE: Zr, Nb, Ta, Hf, U, Th) and rare-earth elements (REE: La to Lu; + Y) were measured with a LASER ablation inductively coupled plasma – mass spectrometer. Increasing pressure from 1.5 to 2.5 GPa at similar temperatures and approximately constant fO_2 increases D_{Rb} but decreases D_{Zr} and D_{Hf} and D_{REE} (D_{La}, D_{Ce}, D_{Pr}). An empirical relationship was observed between D_{Zr} and $(Ti/Al)_{M2}$ in the amphibole, which can be described by:

$$\text{Log } D_{Zr} = 0.5323 \times \log (Ti/Al)_{M2} - 1.5924 .$$

Increasing the fO_2 by ~4 log units (~NNO–2.0 to ~NNO + 2.2) at similar temperatures and constant pressure increases D_{Ba} and D_{Nd} but decreases D_{Ti}. An increase in pressure or fO_2 decreases the maximum partition coefficient (D_o), the Young's modulus (E) and the optimum ionic radius (r_o) of the A-, M2- and M4-lattice sites. The calculated r_o values from the monovalent cations (Na, K, Rb) in the A site and the quadrivalent cations (Ti, Hf, Zr) in the M2 lattice sites suggests that amphiboles crystallized from alkaline basalt material have smaller ⟨A-O⟩ and ⟨M2-O⟩, mean bond-lengths than those formed from pargasitic materials at identical pressures and fO_2's. The measured partition coefficients were used to calculate trace element concentrations in melts formed by partial melting of amphibole-bearing peridotite. This modeling demonstrates those changes in either the pressure or fO_2 of melting can exert a significant effect on Rb/HFSE ratios in the melts and thus help explain the wide variations of these ratios sometimes observed in basaltic rock suites.

Introduction

The effects of pressure and oxygen fugacity on partition coefficients (D_i = concentration of *element-i* in crystal/concentration of *element-i* in liquid) between silicate minerals and melts are considered important during petrogenetic modeling. For the amphibole/melt pair there is a general consensus that D decreases with increasing pressure (Green and Pearson 1985; Sweeney et al. 1992; Adam and Green 1994; Fujinawa and Green 1997). However, Adam et al. (1993) observed that D_{Rb} increased by ~2-fold with increasing pressure. Furthermore, Dalpé and Baker (1997) observed ambivalent behavior of D_{Rb} and D_{HFSE} with increasing pressure. In comparison to the significant changes caused by pressure, the effect of oxygen fugacity (fO_2) on $D^{amph/melt}$ is more subtle (Green and Pearson 1985; Adam and Green 1994). Thus there is a need for experimental measurements of partitioning for a large suite of elements to resolve the appropriate relationship between partitioning and variations in pressure and oxygen fugacity.

In this study we report a series of experiments performed at high pressures and at two oxygen fugacities using two different basaltic materials. For each experi-

C. Dalpé (✉)
Department of Earth and Planetary Sciences,
McGill University, Montreal, Quebec H3A 2A7, Canada
e-mail: claude.dalpe@bristol.ac.uk
Tel.: + 44-(0)117-9545409; Fax: + 44-(0)117-9253385

Don R. Baker
Department of Earth and Planetary Sciences,
McGill University, Montreal, Quebec H3A 2A7, Canada

Present address:
CETSEI/EU Geochemical Facility,
Department of Earth Sciences, University of Bristol,
Wills Memorial Building,
Queen's Road, Bristol BS8 1RJ, UK

Editorial responsibility: T. L. Grove

ment, a consistent data-set for 29 elements including 23 trace elements was determined by electron microprobe (EMP) and LASER ablation inductively coupled plasma – mass spectrometer (LA-ICP-MS) analysis. The large data set obtained for *D*'s was used to establish the effect of pressure and oxygen fugacity on the calculated Young's modulus (E) and the optimum radius (r_o) of the amphibole lattice-sites using the model developed by Blundy and Wood (1994). Furthermore, results of these partitioning experiments allow the investigation of the effects of changes in pressure and oxygen fugacity on the trace element concentrations in alkaline basalts produced by partial melting of an amphibole-bearing peridotite source.

Experimental procedures

Starting material

Three starting materials were used to evaluate if pressure and oxygen fugacity significantly affect partition coefficients. These materials were grouped into two bulk compositions: pargasitic and alkaline basalt materials with different major, minor and trace element concentrations. The first group included a pargasite crystal and a pargasitic glass (P-MT and P-MTg respectively, both referred as pargasitic material hereafter; Table 1). The handpicking and preparation of both materials have been described elsewhere (Dalpé et al. 1995). The P-MT material did not receive a premelting process as described in Dalpé et al. (1995) for P-MTg. The second group consisted of an alkaline basalt (FM10) from north of Keauhou, Hawaii (donated by H.S. Yoder Jr.). The alkaline basalt material (FM10) was chosen to coincide with the range of basaltic compositions used in previous amphibole-melt partitioning experiments (Nicholls and Harris 1980; Green and Pearson 1985; Adam et al. 1993; Adam and Green 1994; LaTourrette et al. 1995; Fujinawa and Green 1997). The choice of the pargasitic material was based on its capacity to produce large amphibole crystals at the conditions used in this study.

Experimental techniques

Conditions were chosen to simulate the range of pressure and oxygen fugacity observed in the upper mantle at which amphibole is stable and a liquidus or near-liquidus phase. Capsules were surrounded by pyrophyllite and experiments performed in a piston-cylinder apparatus (Boyd and England 1960) with NaCl-Crushable Alumina-Pyrex furnace assemblies. Experiments at 1.5 GPa were performed with a 1.91-cm assembly (Hudon et al. 1994) and those at and above 2.2 GPa were performed with a 1.27-cm assembly (Dunn 1993). For the experimental conditions and furnace assembly used in this study, a pressure correction of −12.5 and 0% were applied for the 1.91- and 1.27-cm diameter furnace assemblies respectively, based on a pressure calibration with NaCl melting curve following Bohlen's technique (Bohlen 1984).

Temperature was measured with $W_{95}Re_5/W_{26}Re_{74}$ (type-C) thermocouples and no corrections were applied for the effect of pressure on the electromotive force. Experiments were performed in different ways for the 1.91- and 1.27-cm assemblies. For 1.5 GPa experiments (1.91-cm assembly), pressure and temperature were simultaneously increased to 1.7 GPa and 1200 °C respectively. After reaching 1.7 GPa, 1200 °C, pressure was decreased slowly to 1.5 GPa. The samples were held at these conditions for 1 h to totally melt the sample then isobarically cooled at 1 to 10 °C/min to the desired run temperature. For higher pressure experiments in the 1.27 cm assembly the pressure was initially increased to 0.2 GPa over the run pressure (e.g. 2.4 and 2.7 for the 2.2 and 2.5 GPa run pressures respectively). The samples then were isobarically heated to 1200 or 1225 °C (depending on bulk composition) for 1 h to totally melt the starting materials. Samples were then cooled at 10 °C/min and pressure was allowed to fall to the desired run conditions. At the final run temperature, a little adjustment (±5%)

Table 1 Starting materials. *n* Number of analyses; *nd* not determined; *blld* concentration below the lower limit of detection

Starting material	P-MT	P-MTg[a]	FM10[b]
Composition	Pargasite crystal	Pargasitic glass	Alk.-basalt
	$n = 25$	$n = 30$	$n = 30$
SiO_2	39.19 (0.35)	40.43 (0.25)	47.37 (0.19)
TiO_2	3.61 (0.08)	3.81 (0.04)	2.25 (0.05)
Al_2O_3	14.46 (0.24)	14.77 (0.09)	14.58 (0.12)
Fe_2O_3	nd	1.56[c]	1.69[c]
FeO	nd	7.37[c]	9.20[c]
FeO_t[d]	9.11 (0.19)	8.77 (0.16)	10.72 (0.19)
MnO	0.08 (0.02)	0.09 (0.03)	0.18 (0.02)
MgO	14.33 (0.09)	14.48 (0.09)	9.93 (0.11)
CaO	11.89 (0.09)	12.34 (0.06)	10.33 (0.09)
Na_2O	1.90 (0.04)	1.92 (0.03)	2.80 (0.05)
K_2O	2.22 (0.06)	2.29 (0.03)	0.90 (0.03)
P_2O_5	blld	0.04 (0.04)	0.26 (0.03)
Total	96.79	98.94[e]	99.32[e]
(ppm)	n[f] = 3	$n = 7$	n[f] = 4
Rb	17.6 (0.4)	16.6 (0.5)	23.1 (1.2)
Sr	492 (22)	469 (12)	483 (12)
Y	10.4 (0.2)	10.7 (1.2)	18.8 (0.5)
Zr	47.1 (2.6)	52.7 (1.7)	116.2 (3.6)
Nb	11.7 (0.4)	15.2 (1.8)	23.4 (0.3)
Ba	328 (15)	363 (12)	311 (12)
Hf	2.15 (0.23)	2.26 (0.16)	2.56 (1.32)
Ta	0.82 (0.06)	1.00 (0.07)	4.21 (0.14)
Th	blld	0.20 (0.03)	1.58 (0.17)
U	blld	0.06 (0.01)	0.44 (0.11)
La	3.86 (0.20)	5.78 (0.15)	16.7 (0.4)
Ce	15.4 (0.8)	17.6 (0.7)	41.9 (1.1)
Pr	2.70 (0.19)	2.98 (0.14)	5.46 (0.26)
Nd	14.1 (0.5)	14.9 (0.6)	21.5 (1.4)
Sm	3.79 (0.34)	3.84 (0.21)	4.39 (0.2)
Eu	1.28 (0.04)	1.33 (0.07)	1.58 (0.09)
Gd	3.38 (0.31)	4.07 (0.47)	4.61 (0.40)
Tb	0.50 (0.05)	0.50 (0.04)	0.71 (0.03)
Dy	2.52 (0.26)	2.58 (0.14)	3.95 (0.19)
Ho	0.38 (0.06)	0.44 (0.02)	0.77 (0.07)
Er	0.98 (0.12)	1.06 (0.05)	2.31 (0.25)
Tm	0.12 (0.01)	0.13 (0.01)	0.30 (0.04)
Yb	0.66 (0.08)	0.71 (0.04)	1.76 (0.15)
Lu	0.06 (0.01)	0.09 0.01)	0.26 (0.03)

[a] Analyses taken from Dalpé et al. (1995)
[b] Sample analyses were done on glass formed by melting the bulk powder on Pt-loop at T = 1300 °C at FMQ oxygen fugacity in a 1 atm furnace for 4 h
[c] Fe_2O_3 and FeO proportions are calculated using total iron from the electron microprobe at T = 1400 °C (P-MTg) or 1300 °C (FM10), P = 1 atm, and fO_2 = FMQ (Kress and Carmichael 1991)
[d] Total iron as FeO
[e] Totals are calculated using FeO_t
[f] Analyses were performed using a 266nm-Nd:YAG-LASER (model: LUV266X / MiniLase II-20 Hz from New Wave Research Co. Ltd., USA) attached to a quadrupole ICP-MS (model: PlasmaQuad-3 + S-option from TJA Solutions Ltd., UK) at the Department of Earth Sciences, University of Bristol (Bristol, UK). Values in parentheses are based on one standard deviation from multiple analyses in this and subsequent tables (1 σ)

of the final pressure was needed for some runs. During all experiments pressure was maintained within 0.05 GPa of the desired value. Quenching of all experiments was done by cutting off the power resulting in cooling rates of ~200 °C/s.

After each experiment, capsules were opened and some of the run products mounted in oil for optical examination. Run products were then mounted in an epoxy resin and polished before EMP and LA-ICP-MS analyses.

Oxygen fugacities in experiments

Different capsule assemblies were used to create low and high oxygen fugacity conditions. For low oxygen fugacity experiments, mixtures of the starting powders (~12 mg) plus 8–12 wt% deionized water were enclosed in graphite capsules (OD = 2.60, ID = 2.10 and length = 2.90 mm) and covered with a graphite lid. The graphite capsules were then inserted into $Ag_{50}Pd_{50}$ or $Au_{75}Pd_{25}$ capsules (with OD = 3.00, ID = 2.70 and length = 9.00 mm) with graphite powder carefully packed above and below. The outer capsule was crimped and welded in a water bath to eliminate water loss during welding. The oxygen fugacity inside the capsules was determined in an experiment at 1.5 GPa and 1100 °C for 20 h using $Ag_{50}Pd_{50}$ as the outer container with a starting material of FeO (V.T. Baker-analyzed reagent, Lot no. 785176) plus 10 wt% deionized water. X-ray powder diffraction of the run products demonstrated that the oxygen fugacity was in the wüstite field (FeO), which corresponds to at least 2.0 log units below the NNO buffer at those conditions (NNO-2.0). For all experiments performed using this assembly, the estimated Fe^{3+}/Fe^{2+} ratio was assumed to be 0. The second assembly used a single container to produce the high oxygen fugacity, mixtures of starting materials (~20 mg) plus ~10 wt% deionized water were enclosed in $Au_{75}Pd_{25}$ (OD = 3.00, ID = 2.70 and length = 9.00 mm) and welded closed without water loss. The oxygen fugacity inside this assembly was determined to be 2.2 log units above the NNO buffer (NNO + 2.2) at 1.5 GPa, 1220 °C using P-MTg as the starting material (i.e. P-MTg powder +10 wt% deionized water). The value was calculated using analysis of the run products, which consisted of olivine + quenched glass and assuming a Fe^{2+}–Mg exchange coefficient between olivine and melt of 0.34 [i.e. $K_D^{Fe2+/Mg} = (Fe^{2+}/Mg)_{olivine}/(Fe^{2+}/Mg)_{melt} = 0.34$; Ulmer 1989]. The estimated Fe^{3+}/Fe^{2+} ratio calculated in the melt was 0.745. Combining this measurement with the Kress and Carmichael (1991) relationship between fO_2 and the Fe^{3+}/Fe^{2+} yields an oxygen fugacity of NNO + 2.2. Using a similar NaCl-Pyrex assembly, Kawamoto and Hirose (1994) estimated an oxygen fugacity of about 1.3 log units above NNO for an experiment at 0.5 GPa, 1100 °C using $Au_{75}Pd_{25}$.

Iron loss

The estimated iron-loss for the graphite + $Ag_{50}Pd_{50}$ double capsules was calculated by mass-balance to be less than 14 relative% for all run conditions and durations. However, in the one double capsule experiment with an $Au_{75}Pd_{25}$ outer capsule iron loss was high, ~55 relative%, resulting in a zoned amphibole in this experiment (P-MT-34, discussed below). For the single $Au_{75}Pd_{25}$ capsules the estimated iron-loss were less than 10 relative% for all run conditions and durations.

Analytical techniques

Major and minor element analyses

Major and minor elements were analyzed with a JEOL 8900 electron microprobe at the Department of Earth and Planetary Sciences, McGill University. The electron microprobe operated at an accelerating potential of 15 kV with a beam current of 10 nA; for each element, counting times were 20 s on the peak and 10 s on each background position. Albite (Na), diopside (Si, Ca, Mg), andradite (Fe), orthoclase (K, Al) and pyrophanite (Mn, Ti) were used as standards for both minerals and glasses. For both phases (i.e. crystal and glass) a defocused beam with a diameter of 10 μm was used. The beam was defocused because the texture found in the hydrous basaltic glass run products contained < 5 μm anhedral to euhedral spinfex-textured crystals formed during quenching. For each individual micro-spinifex-textured glass, multiple analyses were necessary with the electron microprobe to obtain a representative liquid composition. We calculated a Na-loss during analysis of ~14% relative based on an experiment performed at 1.5 GPa, 1220 °C, 48 h, using hydrated pargasitic glass as starting material enclosed in an $Au_{75}Pd_{25}$ outer capsule. However, this value is normally less than the relative standard deviation value of Na analyses of glasses.

Trace element analyses

LA-ICP-MS analyses were performed with a Fisons VG PQ2+ quadrupole ICP-MS mass spectrometer equipped with a Fisons VG LASER microprobe at the Département de Géologie, Université de Montréal. The LASER is a 1064-nm Spectron SL-282 Nd:YAG with a 350-mJ maximum output pulsed LASER width of 5 ns. All analyses were performed with the LASER in free-running mode; the different parameters and the protocol have been described previously (Dalpé et al. 1995). Trace element concentrations were determined for both minerals and glasses using a matrix-matched in-house basaltic glass (HF-13) as the external standard. Our previous study has shown that partition coefficients measured between amphibole/basanitic quenched melt using this external standardization agree within two standard deviations of *D*'s derived from the synchrotron X-ray fluorescence microprobe analyses on the same run products (Dalpé et al. 1995).

Because the concentrations of heavy-rare-earth elements (HREE), ^{232}Th and ^{238}U in the amphibole run products were very low, three element menus were used to optimize counting statistics. The LILE (^{85}Rb, ^{88}Sr, ^{137}Ba) + HFSE (^{90}Zr, ^{93}Nb, ^{181}Ta, ^{178}Hf, ^{238}U, ^{232}Th) + light-rare-earth elements (LREE: ^{139}La, ^{140}Ce, ^{141}Pr, ^{146}Nd, ^{147}Sm, ^{151}Eu) + ^{89}Y were grouped together to form the first element menu. The middle-rare-earth elements (MREE: ^{151}Eu, ^{159}Tb, ^{160}Gd, ^{163}Dy, ^{165}Ho, ^{166}Er) formed the second group and HREE (^{166}Er, ^{169}Tm, ^{172}Yb, ^{175}Lu) + ^{232}Th and ^{238}U formed the third group. In the three menus, ^{44}Ca was used as the internal standard and replicate isotopes were used to monitor reproducibility between different element acquisition menus (e.g. Eu, Er, Th, U). The acquisition time for one complete analysis was fixed at three repetitions of 45 s for a total time of 135 s. The total counting time used by the detector for each mass during one complete analysis was between ~2 and 5 s for the 17 or 7 isotopes in the different element menus respectively. Based on counting statistics the calculated lower limits of detection are (in ppm): Rb(0.5), Sr(0.6), Ba(0.1), Zr(1.3), Nb(0.6), Ta(0.03), Hf(0.15), U(0.04), Th(0.08), La(0.09), Ce(0.06), Pr(0.07), Nd(0.08), Sm(0.03), Eu(0.04), Tb(0.07), Gd(0.04), Dy(0.06), Ho(0.07), Er(0.14), Tm(0.06), Yb(0.08), Lu(0.04) and Y(0.5) (calculated following Dalpé et al. 1995).

Run products

General observations

The conditions and results of the individual experiments are listed in Table 2. For most starting materials used in this study, large amphiboles (~400–1000 μm along their longest axis) were relatively easy to crystallize. As can be seen in Table 2, run products were identical (P-MTg-43 vs P-MTg-41) or very similar (P-MT-27 vs P-MT-34, P-MTg-12 vs P-MT-34 and FM10-23 vs FM10-25) for

Table 2 Experimental conditions and run products. *cap. assemb*. Capsule assembly; *am* amphibole; *mi* mica; *ol* olivine; *cpx* clinopyroxene; *ilm* ilmenite; *gl* glass; *AgPd+g*-$Ag_{50}Pd_{50}$ + graphite inner capsules assembly; *AuPd+g*-$Au_{75}Pd_{25}$ + graphite inner capsules assembly; *AuPd*-$Au_{75}Pd_{25}$ capsule assembly

Starting material	Run no.	T (°C)	P (GPa)	Cap. assemb.	fO_2[a]	H_2O[b] (wt%)	Time (h)	Modes[c]					
								am	mi	ol	cpx	ilm	gl
P-MT	27	1100	1.5	AgPd + g	Low	10	100	62	9	tr	11	–	18
P-MT	34[d]	1050	2.5	AuPd + g	Low	10	72	20	8	–	16	–	56
P-MTg	12	1100	1.5	AgPd + g	Low	8	24	48	5	tr	7	–	40
P-MTg	43	1050	1.5	AuPd	High	10	24	24	3	8	2	–	63
P-MTg	41	1075	2.5	AuPd	High	10	24	8	10	3	14	–	65
FM10	02	1040	1.5	AgPd + g	Low	10	24	21	6	–	–	–	73
FM10	23	1000	1.5	AuPd	High	10	100	27	–	–	14	–	59
FM10	25	1000	2.2	AuPd	High	10	100	48	–	–	13	1	38

[a] Low oxygen fugacity buffer using the graphite inner capsule with $Ag_{50}Pd_{50}$ or $Au_{75}Pd_{25}$ and high oxygen fugacity buffer using a single capsule of $Au_{75}Pd_{25}$ alloy; the log fO_2 determined inside these containers were found to be NNO + 2.2 and NNO−2.0 respectively
[b] Total weight percent of deionized water added to the charge
[c] Modes are calculated by least-square mass-balance using SiO_2, TiO_2, Al_2O_3, FeO, MgO, CaO, Na_2O, and K_2O from electron microprobe analyses normalized to 100%
[d] Zoned amphibole was observed for this run. None of these run products appeared water saturated

the four pairs of experiments performed at the low and high pressures using a fixed oxygen fugacity. However, for the four pairs of experiments performed at a fixed run pressure but at different oxygen fugacities, run products were not always similar. The maximum pressure of amphibole stability in the alkaline basalt (FM10) was located between 2.2 and 2.5 GPa at NNO + 2.2. Thus, the highest run pressure investigated was 2.2 GPa instead of 2.5 GPa as used for P-MT and P-MTg materials. We did not have success in crystallizing large amphiboles for trace element analyses from FM10 at 2.2 GPa and low oxygen fugacity (NNO-2.0).

In addition to amphibole and glass, crystals of phlogopite, pyroxene and olivine were found in some experiments and analyzed for major elements (see Dalpé 1998). Phlogopites were always euhedral and in contact with glass. Pyroxenes were frequently anhedral and surrounded by either amphibole or mica, although some were euhedral and in contact with the glass. Olivine was always anhedral and surrounded by either pyroxene or amphibole. No trace element analyses of these phases were made because of either their small dimensions or their apparent disequilibrium with the melt.

Amphibole

The major and trace element analyses of amphiboles are listed in Table 3. All of the amphiboles from this study are calcic amphiboles according to Leake et al.'s (1997) classification based on 23 atoms of oxygen per formula unit (apfu). They consist of pargasites (P-MT-34a, P-MT-34b, P-MTg-41, FM10-23, FM10-25) or titanian pargasites (P-MT-27, P-MTg-12, P-MTg-43 and FM10-02).

Cation site occupancies of major and minor elements in amphibole (e.g. Si, Ti, Al, Cr, Fe^{2+}, Fe^{3+}, Mn, Mg, Ca, Na, K) are well established (e.g. Hawthorne 1983; Della Ventura et al. 1991; Paris et al. 1993; Hawthorne et al. 1995, 1996; Jenkins et al. 1997; Leake et al. 1997; Oberti et al. 1998; Ventura et al. 1998). The general consensus for the cation site-assignments in calcic amphibole (pargasite, titanian pargasite, or kaersutite) are:

^{XII}A: K^+, Na^+
$^{VIII}M4$: Na^+, Ca^{2+}, Mn^{2+}, Fe^{2+}, Mg^{2+}
$^{VI}M1$: Mn^{2+}, Fe^{2+}, Mg^{2+}
$^{VI}M2$: Ti^{4+}, Al^{3+}, Fe^{3+}, Cr^{3+}
^{IV}T: Si^{4+}, Al^{3+}

Note that no distinction is made in this study between the different cavities in the A site (i.e. A2, Am, A2/m), between the $^{VIII}M4$ and $^{VI}M4'$ sites, between the M1 and M3 sites and between the T1 and T2 sites (referred hereafter as A, M4, M1 and T sites respectively). Furthermore for pargasite and kaersutite compositions, the A site may only be partially filled by Na and/or K. The estimated proportion of Fe^{3+} in amphibole is based on the empirical model of Schumacher (1997).

The site occupancies for trace elements (LILE, HFSE, REE) are not well established compared to major and minor elements and few studies have reported direct observation (Della Ventura and Robert 1990; Robert et al. 1993; Brumm et al. 1998; Tiepolo et al. 1998a; Foley et al. 1999). However, trace element site occupancies for amphibole (and many other silicate minerals) are largely structurally controlled by relationships between partition coefficients, ionic radii and ionic charges (Jensen 1973; Möller 1988; Liu et al. 1992; Robert et al. 1993; Brenan et al. 1995; LaTourrette et al. 1995; Klein et al. 1997; Tiepolo et al. 1998a; Foley et al. 1999). Based on in-situ and partitioning studies the trace element site-occupancies in pargasite and Ti-rich pargasite can be summarized as: Rb^+ and Ba^{2+} in the ^{XII}A site; REE^{3+}, Y^{3+} and Sr^{2+} in the $^{VIII}M4$ site; Nb^{5+} and Ta^{5+} in the $^{VI}M1$ site and Zr^{4+} and Hf^{4+} in the $^{VI}M2$ site. We assumed that all the REE + Y partition into the $^{VIII}M4$ site without distinction between M4 and M4′

Table 3 Amphibole compositions in experiments. $Fe^{3+/2+}$ Calculated Fe^{3+}/Fe^{2+} ratio (Schumacher 1997)

Starting material	P-MT	P-MT[a]	P-MT[a]	P-MTg	P-MTg	P-MTg	FM10	FM10	FM10
Run no.	27	34a	34b	12	41	43	02	23	25
	n = 30	n = 25	n = 12	n = 30	n = 34	n = 30	n = 27	n = 22	n = 19
SiO_2	40.65 (0.64)	41.28 (0.52)	42.59 (0.38)	40.23 (0.60)	40.90 (0.53)	40.23 (0.59)	43.42 (0.49)	42.25 (0.27)	41.60 (0.45)
TiO_2	3.56 (0.16)	2.13 (0.11)	2.12 (0.05)	3.78 (0.22)	1.79 (0.15)	3.19 (0.23)	2.59 (0.17)	2.17 (0.09)	1.66 (0.03)
Al_2O_3	15.46 (0.56)	16.05 (0.67)	15.43 (0.41)	16.18 (0.40)	15.93 (0.29)	15.41 (0.50)	11.89 (0.53)	13.72 (0.33)	14.54 (0.20)
FeO	4.98 (0.20)	5.03 (0.46)	2.50 (0.08)	5.15 (0.30)	4.67 (0.15)	5.79 (0.57)	8.06 (0.37)	8.80 (0.32)	11.94 (0.33)
MnO	blld	blld	blld	blld	blld	blld	0.12 (0.02)	0.11 (0.03)	0.15 (0.02)
MgO	16.29 (0.37)	16.99 (0.26)	18.50 (0.16)	16.27 (0.24)	17.27 (0.31)	16.40 (0.55)	16.73 (0.35)	15.95 (0.31)	13.59 (0.31)
CaO	11.86 (0.18)	11.21 (0.30)	11.69 (0.08)	12.08 (0.25)	12.23 (0.19)	12.50 (0.11)	10.67 (0.35)	10.75 (0.19)	10.11 (0.11)
Na_2O	2.13 (0.18)	2.14 (0.17)	1.91 (0.04)	1.86 (0.09)	1.80 (0.10)	1.86 (0.08)	3.05 (0.10)	2.74 (0.06)	2.77 (0.05)
K_2O	1.83 (0.25)	2.22 (0.24)	2.54 (0.05)	2.21 (0.12)	2.77 (0.08)	2.38 (0.12)	1.15 (0.12)	1.06 (0.06)	1.08 (0.04)
Total	96.76	97.05	97.27	97.76	97.36	97.76	97.68	97.55	97.44
$Fe^{3+/2+}$	0.00	0.00	0.00	0.00	0.90	0.24	0.00	0.00	0.00
(ppm)	n[b] = 6–12	n = 2–6	n = 1	n = 3–13	n = 1–4	n = 3–7	n = 6–12	n = 6–12	n = 2–8
Rb	5.16 (1.25)	4.19 (0.35)	nd	5.16 (1.23)	6.73 (0.003)	6.22 (1.33)	5.48 (1.28)	6.23 (0.62)	8.69 (0.66)
Sr	336.8 (16.4)	214.8 (20.0)	nd	343.0 (14.9)	277.7 (3.6)	379.6 (28.9)	430.9 (24.5)	216.4 (13.0)	201.9 (7.1)
Y	6.81 (0.47)	4.89 (0.26)	nd	6.77 (0.50)	4.97 (0.16)	6.90 (0.41)	11.5 (1.6)	12.5 (0.6)	14.6 (0.4)
Zr	15.1 (1.5)	5.13 (0.44)	nd	16.4 (1.2)	5.67 (0.04)	20.8 (0.70)	85.0 (13.2)	22.3 (3.4)	19.1 (1.7)
Nb	2.78 (0.33)	blld	nd	3.08 (0.51)	blld	2.91 (1.02)	18.8 (1.4)	3.20 (0.46)	3.15 (0.94)
Ba	180.2 (26.2)	108.5 (7.1)	nd	175.6 (27.8)	182.0 (3.7)	250.2 (28.3)	57.6 (3.4)	114.8 (11.7)	107.0 (7.2)
Hf	1.05 (0.17)	0.39 (0.03)	nd	1.06 (0.16)	0.19[c]	1.22 (0.07)	2.82 (0.56)	0.86 (0.14)	0.76 (0.09)
Ta	0.17 (0.06)	0.05 (0.01)	nd	0.28 (0.03)	blld	0.26 (0.06)	1.29 (0.08)	0.67 (0.08)	0.57 (0.16)
Th	blld	blld	nd	blld	blld	blld	blld	blld	blld
U	blld	blld	nd	blld	blld	blld	blld	blld	blld
La	1.58 (0.31)	0.39 (0.02)	nd	0.92 (0.16)	0.59 (0.09)	1.44 (0.33)	6.97 (0.80)	2.02 (0.48)	1.90 (0.31)
Ce	6.74 (1.09)	1.97 (0.18)	nd	4.27 (0.52)	2.88 (0.01)	6.51 (0.94)	24.4 (2.0)	7.76 (1.11)	8.03 (0.74)
Pr	1.39 (0.14)	0.55 (0.06)	nd	0.99 (0.12)	0.68 (0.02)	1.39 (0.19)	4.13 (0.33)	1.45 (0.10)	1.58 (0.14)
Nd	7.48 (0.65)	3.39 (0.28)	nd	6.16 (0.27)	4.57 (0.14)	8.04 (0.69)	20.3 (1.7)	8.39 (0.97)	8.33 (0.48)
Sm	2.18 (0.24)	1.30 (0.16)	nd	1.91 (0.28)	1.41 (0.03)	2.53 (0.16)	5.55 (0.92)	2.34 (0.29)	2.71 (0.23)
Eu	0.88 (0.19)	0.74 (0.13)	1.10	0.89 (0.08)	0.56 (0.09)	0.97 (0.05)	1.86 (0.23)	1.01 (0.11)	1.04 (0.16)
Gd	2.00 (0.50)	1.60 (0.28)	1.78	2.47 (0.16)	1.73 (0.07)	2.56 (0.06)	4.75 (0.24)	2.93 (0.25)	3.36 (0.29)
Tb	0.30 (0.08)	0.24 (0.01)	0.26	0.33 (0.04)	0.26 (0.01)	0.34 (0.02)	0.65 (0.05)	0.47 (0.03)	0.51 (0.02)
Dy	1.43 (0.37)	1.23 (0.12)	1.18	1.73 (0.12)	1.18 (0.03)	1.66 (0.03)	2.86 (0.17)	2.65 (0.14)	2.87 (0.24)
Ho	0.22 (0.06)	0.25 (0.004)	0.21	0.29 (0.04)	0.19 (0.01)	0.29 (0.01)	0.43 (0.02)	0.50 (0.02)	0.53 (0.03)
Er	0.59 (0.16)	0.51 (0.07)	0.67	0.78 (0.07)	0.47 (0.04)	0.72 (0.08)	1.10 (0.32)	1.28 (0.13)	1.63 (0.18)
Tm	blld	blld	nd	0.10 (0.01)	blld	0.08 (0.01)	0.14 (0.03)	0.12 (0.01)	0.23 (0.03)
Yb	0.40 (0.13)	0.34 (0.10)	nd	0.47 (0.05)	0.24 (0.06)	0.51 (0.01)	0.72 (0.26)	0.77 (0.03)	1.34 (0.10)
Lu	blld	blld	nd	0.09 (0.01)	0.05 (0.01)	0.06 (0.01)	0.06 (0.01)	0.12 (0.02)	0.17 (0.01)

[a] Zoned amphibole observed in run products
[b] Number of analyses vary as function of the different acquisition menus and replicate isotopes
[c] Single analysis

as proposed by Tiepolo et al. (1998b) and Bottazzi et al. (1999) because of the absence of accurate structure refinements. Furthermore, we did not observe any evidence of D_{REE} site splitting as proposed by Bottazzi et al. (1999).

We checked major element homogeneity of the different synthesized amphibole crystals by performing line traverses and calculating the relative standard deviation (RSD) for each set of multiple analyses. The average RSD gave: SiO_2 (1.23%), TiO_2 (5.4%), Al_2O_3 (3.0%), FeO (4.5%), MgO (1.9%), CaO (2.0%), Na_2O (3.8%) and K_2O (8.0%) respectively. These average RSD values were all less than 10%, suggesting homogeneity in major elements. For the trace elements we have calculated the average RSD based on multiple analyses of each amphibole run product. The minimum and maximum average RSDs for the trace element concentrations range from 5 to 19% for Sr and Yb respectively. The higher average RSD's attached to Yb and other incompatible elements are related to the low concentrations measured by the LA-ICP-MS in the amphibole. All of these relative standard deviations are similar to those expected from counting statistics and indicate the homogeneity of the experimental amphiboles.

Equilibrium aspect of amphibole run products

Our experiments demonstrate that constant partitioning between amphibole and liquid seems to be reached within 20 h. Figure 1 shows the variation of partition coefficient for Sr and Y as a function of the duration of experiments performed at 1.5 GPa and 1100 °C. As shown in this figure, constant partition coefficients are reached within 20 h based on one standard deviation or within 10 h based on two standard deviations. All ex-

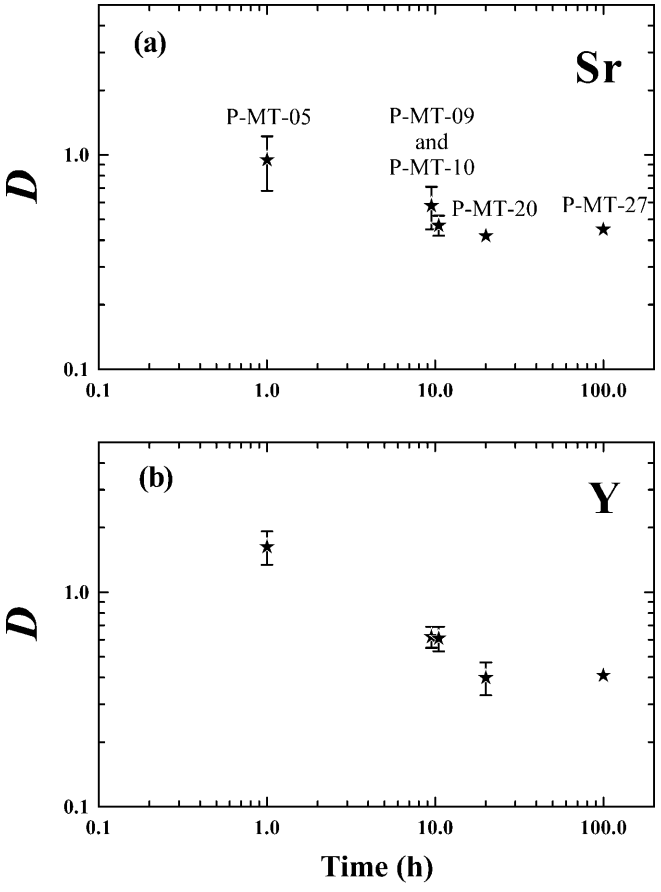

Fig. 1 Variation of partition coefficients (*D*) as a function of the run duration. The analyses of P-MT-05 (1 h), P-MT-09 (10 h), P-MT-10 (10 h), and P-MT-20 (20 h) runs were performed by synchrotron X-ray-fluorescence microprobe (SXRFM) on X26A beamline at the National Synchrotron Light Source at Brookhaven National Laboratory (Upton, New York) (Dalpé et al. 1992, 1995). Note that both P-MT-09 and P-MT-10 had the same run duration, 10 h, but were plotted apart for better clarity. The experiments P-MT-05, P-MT-09, P-MT-10, and P-MT-20 are not listed in Table 2 and subsequent tables because of their non-equilibrium nature (P-MT-05, P-MT-09, P-MT-10) or the inability to analyze the amphibole run products by LA-ICP-MS because of their small size (P-MT-20). Standard deviations smaller than the symbol size are not shown in this and subsequent figures

periments reported in this study were all greater than 20 h duration.

As mentioned previously, zoned amphibole was observed in the P-MT-34 run. All the amphiboles from this run product contained a Fe-rich core surrounded by a 10- to 50-μm thick rim of a Fe-poor composition (P-MT-34a and P-MT-34b respectively; Table 3). Because of the small size of the Fe-poor zone, we were limited to performing a single analysis in this zone by LA-ICP-MS (i.e. the MREE acquisition menu: Eu, Gd, Tb, Dy, Ho, Er; Table 3). All other LA-ICP-MS analyses were performed in the Fe-rich core.

Despite the zoning we believe that useful constraints on the effects of pressure and oxygen fugacity controls on trace element partitioning can still be extracted from this experiment because (1) each zone is homogeneous in major elements; (2) the trace element concentrations (MREE) between both zones are within, or close to, two standard deviations (Table 3); (3) the RSD values attached to the trace elements in the Fe-rich zone has the same range as those measured on other amphibole run products; and (4) the *D* values associated with the MREE from both zones are within or close to one standard deviation of each other when we propagate the analytical uncertainties. We will consider only the Fe-rich core zone (P-MT-34a) for the rest of this study.

Variations in amphibole compositions with increasing pressure at a fixed oxygen fugacity

The variation in major element concentrations in the amphibole run products from the pairs of experiments shows an increase in Al_{M2}, K_A and Al_T/Al_{M2} and a decrease in Ti_{M2} with Ca_{M4} as we increased pressure. Furthermore, with increasing pressure, the Fe_{total} in the M1-M2 sites decreased for amphiboles in the P-MT and P-MTg experiments whereas it increased in the FM10 experiments. For all experiments the Mg behaved inversely to Fe_{total} in the M1-M2 sites of the amphiboles.

Based on two standard deviations from multiple analyses for experiments performed at the low oxygen fugacity, concentrations of Sr, Nb, Zr, Hf, Y, La, Ce, Pr and Nd decrease in the P-MT amphiboles with increasing pressure (Table 3). For experiments performed at higher oxygen fugacity using the P-MTg material, the concentrations of Ba, Sr, Nb, Ta, Zr, Hf, Y, La, Ce, Pr, Nd, Sm, Eu, Gd, Tb, Dy, Ho, Er and Yb also decreased with increasing pressure. Adam and Green (1994) and Fujinawa and Green (1997) observed similar trends for trace element concentrations in their amphibole run products. However, there is little variation in trace element concentrations for the amphiboles formed in alkaline basalt experiments performed at the high oxygen fugacity. In these experiments, La decreases while Y, Tm and Yb increase in the amphibole with increasing pressure.

Variation in amphibole compositions with increasing oxygen fugacity at a fixed pressure

The variation in major element concentrations in amphibole run products from the four pairs of experiments shows an increase of Al_T and Ca_{M4} whereas Ti_{M2} decreases with increasing oxygen fugacity. Moreover, but not surprisingly, the estimated Fe^{3+}/Fe^{2+} ratio in the amphibole produced from the P-MTg material increases as the oxygen fugacity increases (Table 3). Adam and Green (1994) observed the same trend for Ti_{M2} and for Fe^{3+}/Fe^{2+} in amphibole run products with increasing oxygen fugacity. Surprisingly, the Fe^{3+}/Fe^{2+} ratio trend was not observed in the amphiboles crystallized from the FM10 material because of the absence of any estimated

Fe^{3+}. Other variations observed for the pargasitic materials obtained at both pressures were an increase in K_A and a decrease in Al_{M2}, $Fe^{2+}{}_{M4}$ with increasing oxygen fugacity. In amphiboles crystallized from the alkaline basalt, Al_{M2} and $Fe^{2+}{}_{M4}$ increased whereas K_A decreased with increasing oxygen fugacity. The opposite behavior of the Mg# in amphiboles crystallized from the pargasitic composition compared to the alkaline basaltic material might be an artifact caused by the empirical estimation of the Fe^{3+}/Fe^{2+} ratio in FM10s experiments.

No systematic variation in trace element concentrations, at the two standard deviation level, was observed as we increased fO_2 in the four different pairs of experiments.

Glass

Major and trace element analyses of glass run products are listed in Table 4. We checked the homogeneity of the synthesized quenched glass in all experiments by performing line traverses across it and calculating the RSD from the multiple analyses. The average RSDs calculated from different analyses in glass typically gave SiO_2 (3.75%), TiO_2 (5.2%), Al_2O_3 (5.5%), FeO (6.9%), MgO (13%), CaO (8.3%), Na_2O (20%) and K_2O (20%). The high RSDs calculated for most elements in the glass compared with amphibole were attributed to micro-spinifex quench crystal formation. For the trace elements the minimum and maximum average RSDs range from 3 to 12% for Ba and U respectively, suggesting homogeneity. Furthermore, because LA-ICP-MS analyzed a larger volume of the sample compared with the electron microprobe, no significant differences were observed in the average RSD values attached to the trace elements measured in the different micro-spinifex glasses.

In summary, it appears that the different quenched glasses (referred hereafter as melt) and the amphibole run products were homogeneous in major, minor and trace elements. Furthermore, because of the long-run durations used in this study (≥20 h), partitioning of major, minor and trace elements between amphibole and melt demonstrate steady state, if not equilibrium, behavior at run conditions.

Partition coefficients

In order to compare our partition coefficients with previous experimental work we calculated the average partition coefficients (i.e. D_i^{avg}) of each bulk material independently of pressure, oxygen fugacity and temperature (Fig. 2). The general trends observed in our partition coefficients are similar in shape and agree well with those from previous experimental results (Fig. 2). This might suggest, as proposed by some criteria of Watson's (1985) study, that partition coefficients show an adherence to Henry's law at concentration levels ranging from sub-ppm to ppm (e.g. LILE, HFSE, REE) to as high as wt% (e.g. K, Ti). Some peaks along the profile (e.g. D_K, D_{Sr} and D_{Ti}) disturb the general trend and suggest that the order of incompatibility generally used for petrological and experimental studies might not be the best order for amphibole partitioning. However, we keep this order to simplify the comparison of partition coefficients with other studies (e.g. Green 1994).

The average ranges observed in partition coefficients between both bulk materials demonstrate that D_{Rb}, D_{Ba} and D_{Sr} are higher for experiments performed with the pargasitic materials than those performed with the alkaline basalt material. However, almost all the partition coefficients measured in this study are similar to, with two standard deviations, of all previous studies (Green and Pearson 1985; Adam et al. 1993; Adam and Green 1994; Dalpé and Baker 1994; Dalpé et al. 1995; LaTourrette et al. 1995; Bottazzi et al. 1999), with the exception of our estimated maximum values of D_{Th} and D_U, which are high compared with those obtained by LaTourrette et al. (1995) and Brenan et al. (1995). The D_{Ti} measured in the experiments using pargasitic this study or a kaersutite materials (Dalpé and Baker 1994; Dalpé et al. 1995) are all incompatible ($D < 1$). However, D_{Ti} measured from experiments using a "basaltic rock composition" as starting material (Nicholls and Harris 1980; Green and Pearson 1985; Adam et al. 1993; Adam and Green 1994; LaTourrette et al. 1995; Fujinawa and Green 1997; including this study with FM10 material) showed a range from incompatible (0.64) to compatible (2.56) at similar experimental conditions. Nicholls and Harris (1980) and Bottazzi et al. (1999, run no. 4722-13a) measured higher D_{Yb} ($0.7 < D_{yb} < 0.9$) compared with less than 0.64 from this and previous studies (Dalpé and Baker 1994; Dalpé et al. 1995; Bottazzi et al. 1999, run no. R352-3).

The effect of pressure on partition coefficients at a fixed oxygen fugacity

Figure 3 shows the effect of pressure on partition coefficients for the two pairs of experiments performed at high fO_2. The effect of pressure on partition coefficients between amphibole and basaltic melt is minor and for most trace elements no measurable effect can be seen at the one standard deviation level. At low oxygen fugacity conditions, we observed that D_{Rb} increases while D_{Nb}, D_{Zr}, D_{Hf}, D_{Ti} and D_{La} decrease with increasing pressure for the experiments at low oxygen fugacity. At high oxygen fugacity D_{Sr}, D_{Ta}, D_{Zr}, D_{Hf}, D_{Ce}, D_{Pr} and D_{Nd} decrease with increasing pressure. Comparison with the alkaline basalt experiments at high oxygen fugacity demonstrates that D_{Yb} and D_{Lu} increase while D_{Ba} and D_{La} decrease with increasing pressure.

The negative relationships observed between D_{Sr}, D_{Zr}, D_{Hf}, D_{Ti}, D_{Ho} and pressure are similar to previous

Table 4 Quenched glass compositions in experiments. $Mg\#_t$ Mg number$_t$ = [100 × Mg/(Mg + Fe_{total})]

Starting material	P-MT	P-MT	P-MTg	P-MTg	P-MTg	FM10	FM10	FM10
Run no.	27	34	12	41	43	02	23	25
	n = 18	n = 10	n = 26	n = 18	n = 16	n = 20	n = 14	n = 17
SiO_2	37.11 (1.43)	34.14 (2.98)	36.59 (1.70)	34.18 (1.83)	37.98 (1.70)	35.92 (1.77)	45.30 (1.78)	47.07 (2.25)
TiO_2	4.07 (0.15)	4.15 (0.40)	3.86 (0.19)	4.46 (0.46)	4.81 (0.19)	2.15 (0.17)	2.25 (0.12)	1.65 (0.13)
Al_2O_3	14.34 (0.66)	14.10 (1.33)	16.75 (2.31)	14.75 (1.20)	15.36 (0.67)	11.64 (0.90)	16.49 (1.04)	16.37 (1.05)
FeO	8.51 (0.43)	3.28 (0.34)	8.55 (0.79)	8.35 (0.66)	8.54 (0.28)	10.45 (0.39)	9.47 (0.89)	8.46 (1.97)
MnO	0.15 (0.03)	0.08 (0.02)	0.13 (0.03)	0.10 (0.02)	0.14 (0.02)	0.25 (0.03)	0.18 (0.03)	0.18 (0.04)
MgO	7.67 (0.90)	11.33 (2.81)	9.35 (1.73)	10.24 (1.23)	8.67 (0.34)	7.14 (0.41)	6.08 (1.17)	3.29 (1.17)
CaO	12.89 (0.72)	10.04 (2.24)	12.44 (1.37)	11.34 (1.24)	12.63 (0.62)	11.06 (1.19)	7.52 (0.81)	7.14 (0.97)
Na_2O	1.55 (0.28)	1.22 (0.39)	1.62 (0.26)	1.56 (0.13)	1.45 (0.21)	3.56 (0.77)	1.70 (0.43)	1.35 (0.60)
K_2O	1.21 (0.24)	1.23 (0.44)	1.39 (0.44)	1.26 (0.26)	1.40 (0.18)	1.63 (0.20)	0.87 (0.27)	0.77 (0.25)
P_2O_5	0.14 (0.05)	blld	0.07 (0.02)	0.04 (0.01)	0.05 (0.02)	2.25 (0.33)	0.26 (0.09)	0.51 (0.12)
Total	87.64	79.59	90.75	86.27	91.03	86.06	90.11	86.79
$Fe^{3+/2+}$ [a]	0	0	0	0.6	0.6	0	0.6	0.6
$Mg\#_t$	62	86	66	69	64	55	53	41
(ppm)	n[b] = 3–12	n = 2–6	n = 2–9	n = 6–12	n = 2—10	n = 4–11	n = 2–8	n = 3–8
Rb	16.1 (0.8)	6.65 (0.57)	15.5 (2.0)	6.46 (1.07)	11.6 (1.2)	25.7 (1.2)	26.6 (2.5)	32.7 (2.1)
Sr	745.1 (16.9)	486.5 (14.8)	661.2 (13.3)	555.5 (18.5)	660.4 (3.3)	1924 (129)	493.6 (18.7)	682.2 (33.3)
Y	16.6 (0.3)	11.2 (0.2)	14.8 (0.5)	13.2 (0.3)	17.1 (0.6)	33.2 (1.9)	19.9 (0.5)	24.4 (0.9)
Zr	96.8 (2.3)	57.3 (2.6)	88.3 (3.1)	70.7 (5.8)	99.1 (3.8)	352.9 (17.3)	142.6 (4.1)	216.6 (9.2)
Nb	34.3 (0.4)	15.1 (1.5)	29.8 (1.1)	20.5 (0.7)	35.0 (1.1)	136.2 (9.6)	31.6 (0.3)	47.9 (1.7)
Ba	428.1 (11.1)	255.8 (4.0)	371.6 (3.5)	253.3 (14.4)	346.6 (4.3)	353.4 (21.0)	339.5 (8.2)	463.2 (17.7)
Hf	3.31 (0.29)	2.16 (0.15)	3.02 (0.25)	2.77 (0.13)	3.53 (0.12)	6.79 (0.27)	3.27 (0.37)	5.11 (0.30)
Ta	2.10 (0.04)	1.11 (0.07)	1.89 (0.08)	1.39 (0.12)	2.26 (0.09)	7.13 (0.43)	5.56 (0.38)	8.61 (0.30)
Th	0.50 (0.05)	0.16 (0.03)	0.37 (0.05)	0.26 (0.03)	0.43 (0.02)	12.4 (0.8)	1.93 (0.15)	3.19 (0.30)
U	0.15 (0.04)	0.09 (0.01)	0.11 (0.01)	0.07 (0.01)	0.11 (0.01)	4.06 (0.34)	0.63 (0.07)	1.04 (0.03)
La	27.1 (1.6)	11.8 (0.4)	11.8 (0.7)	7.79 (0.17)	12.9 (0.3)	112.9 (8.0)	20.4 (0.3)	32.7 (2.1)
Ce	66.7 (3.3)	25.6 (1.4)	35.6 (0.9)	23.9 (0.7)	37.3 (0.8)	216.7 (15.8)	47.3 (1.0)	70.9 (4.0)
Pr	9.13 (0.28)	4.26 (0.17)	5.63 (0.24)	4.06 (0.14)	6.06 (0.13)	25.3 (1.9)	5.73 (0.13)	8.72 (0.69)
Nd	36.3 (0.5)	18.9 (0.5)	25.5 (0.7)	19.6 (0.7)	27.3 (0.6)	93.7 (6.0)	23.5 (0.8)	34.3 (1.4)
Sm	6.41 (0.23)	4.42 (0.20)	6.12 (0.49)	4.61 (0.26)	6.09 (0.09)	17.5 (1.1)	4.57 (0.70)	6.54 (0.34)
Eu	2.06 (0.38)	2.68 (0.04)	2.04 (0.07)	1.65 (0.06)	2.13 (0.05)	5.89 (0.38)	1.72 (0.09)	2.34 (0.23)
Gd	4.38 (0.86)	3.73 (0.13)	5.20 (0.29)	4.42 (0.08)	5.68 (0.10)	14.4 (0.9)	4.88 (0.31)	5.67 (0.23)
Tb	0.60 (0.12)	0.51 (0.01)	0.72 (0.03)	0.61 (0.05)	0.77 (0.01)	1.97 (0.08)	0.72 (0.06)	0.89 (0.01)
Dy	2.88 (0.65)	2.73 (0.08)	3.55 (0.14)	3.14 (0.18)	3.96 (0.12)	8.80 (0.22)	3.90 (0.07)	4.53 (0.46)
Ho	0.49 (0.12)	0.46 (0.01)	0.61 (0.01)	0.55 (0.04)	0.69 (0.03)	1.34 (0.11)	0.74 (0.03)	0.84 (0.02)
Er	1.41 (0.32)	1.14 (0.05)	1.61 (0.11)	1.41 (0.08)	1.81 (0.06)	3.28 (0.21)	2.12 (0.13)	2.62 (0.16)
Tm	0.20 (0.03)	0.14 (0.01)	0.19 (0.02)	0.18 (0.01)	0.24 (0.01)	0.37 (0.02)	0.23 (0.004)	0.41 (0.02)
Yb	1.26 (0.09)	0.86 (0.01)	1.09 (0.01)	1.02 (0.07)	1.48 (0.02)	2.08 (0.32)	1.71 (0.07)	2.45 (0.30)
Lu	0.15 (0.03)	0.10 (0.01)	0.18 (0.02)	0.11 (0.01)	0.16 (0.01)	0.19 (0.02)	0.28 (0.004)	0.32 (0.02)

[a] The Fe^{3+}/Fe^{2+} ratio was calculated using total iron from the electron microprobe at run conditions mentioned in Table 2 (Kress and Carmichael 1991)
[b] Number of analyses vary as function of the different acquisition menus and replicate isotopes

results of Adam and Green (1994) for D_{Sr}, D_{Ti}, D_{Ho} and of Fujinawa and Green (1997) for D_{Zr} and D_{Hf}; however, D_{Rb} shows an opposite behavior. Adam et al. (1993) mentioned a similar behavior of increasing D_{Rb} (two-fold) with increasing pressure (i.e. 1.0 to 2.0 GPa) for experiments performed at similar temperatures using a F-doped basanitic material. The increase in D_{Rb} can also be observed in our experiments with the alkaline basalt material, but remains within one standard deviation (Fig. 3b). This may be the result of the smaller range of pressure used for the FM10 experiments (0.7 GPa) compared with the P-MT and P-MTg experiments (1.0 GPa).

Figure 4 shows the partition coefficient of Zr as a function of the $(Ti/Al)_{M2}$ ratio observed in different amphibole run products with increasing pressure. Increasing pressure directly affects amphibole composition, modifying its partition coefficient. A general empirical equation can be written as:

$$\text{Log } D_{Zr} = 0.4888 \times \log(Ti/Al)_{M2} - 1.6486$$

which can be applied to basaltic systems at upper mantle conditions (coefficient of determination = $R^2 = 0.61$). The F-rich experiments of Adam et al. (1993) were not included in the linear regression because of the effect of fluorine on Ti in the system, which lowers D_{Ti}. Based on the relationship between D_{Zr} and the $(Ti/Al)_{M2}$ ratio obtained in all experiments, oxygen fugacity may possibly influence the partitioning of Zr (compare the 1.5 GPa experiments performed with the alkaline basalt material at the low fO_2 vs the high fO_2; discussed below), but the variations are within one standard deviation for the experiments performed with the pargasitic materials. As mentioned previously, the bulk starting material can

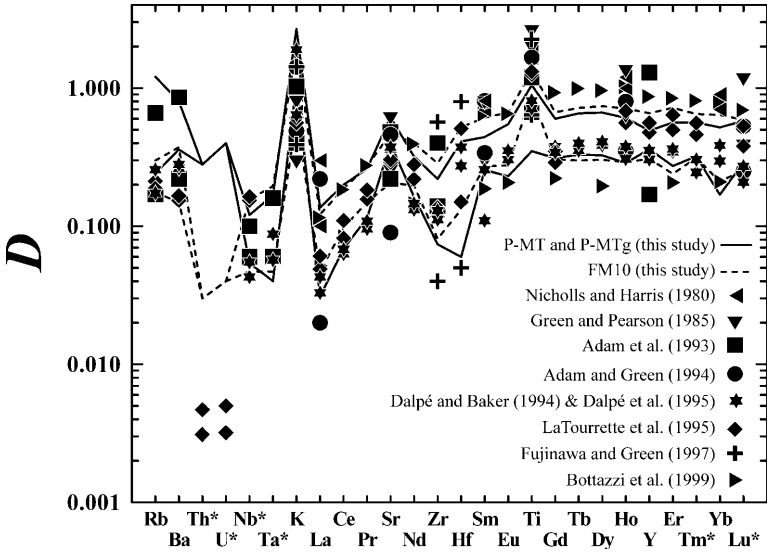

Fig. 2 Minimum and maximum partition coefficients between calcic amphibole and basaltic melt from this and previous studies. The different lines (this study) or symbol ranges (previous experimental studies) were constructed by using minimum and maximum values of one relative standard deviation (1σ) attached to each partition coefficient [i.e. D_i^{min} = minimum value of (D_i–$1\sigma_i$) and D_i^{max} = maximum value of ($D_i + 1\sigma_i$)]. So, in other words, the variations plotted on this figure include ± 1 standard deviation from a single experiment (Dalpé and Baker 1994; Dalpé et al. 1995; LaTourrette et al. 1995) or from multiple experiments performed at different conditions (Nicholls and Harris 1980; Green and Pearson 1985; Adam et al. 1993; Adam and Green 1994; Fujinawa and Green 1997; Bottazzi et al. 1999, run no. 4722-13a and RB52-3; including this study). The areas bounded by the *filled line* and the *dashed line* represent minimum and maximum partition coefficients from this study using the pargasitic and the alkaline basalt materials, respectively. Elements followed by an *asterisk* in this and subsequent figures indicate that for some experiments the partition coefficient (on a qualitative basis) was calculated using the lower limit of detection of the element (i) divided by the concentration of each respective element (i) in the quenched glass [i.e. D_i = lower limit of detection for the element (i) / concentration of the element (i) in the quenched glass; see text and Table 4]. These partition coefficients are maximum values (i.e. $D_{i\text{-max}}$). All previous experiments were performed at a variety of different pressures, temperatures, and oxygen fugacity conditions

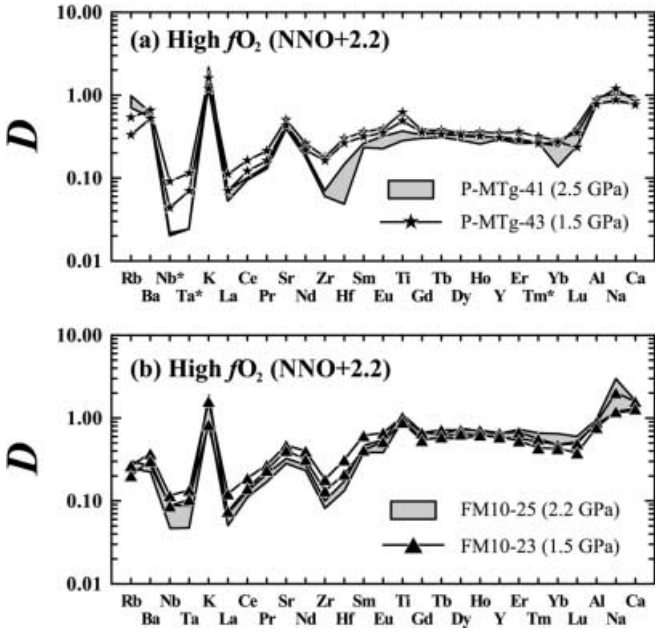

Fig. 3 The effect of pressure on partition coefficients for different oxygen fugacities. **a** Experiments performed with the pargasitic material. **b** Experiments performed with the alkaline basalt material. Variations include one standard deviation from multiple analyses

influence partitioning between an amphibole and basaltic melt for experiments performed at identical pressure and oxygen fugacity and similar temperature (compare the 1.5 GPa experiments using both bulk materials at low or high fO_2). These variations are, however, within (FM10-02 vs P-MTg-12), or close to (FM10-23 vs P-MTg-43), one standard deviation.

The effect of oxygen fugacity on partition coefficients at a fixed pressure

Figure 5 shows the effect of oxygen fugacity on partition coefficients for two different pairs of experiments performed at 1.5 GPa. Increasing the oxygen fugacity from NNO–2.0 to NNO + 2.2 positively affects the partition coefficients of Rb and Ba (LILE) and La and Nd (REE), while it negatively affects Ti, Hf and Zr (HFSE). However, all of these effects are small. Comparing the two different pairs of experiments demonstrates identical behaviors for D_{Ba} and D_{Nd}, which both increase whereas D_{Ti} decreases with increasing oxygen fugacity. Similar trends were observed also for two other P-MT pairs of experiments performed at 1.5 and 2.5 GPa (i.e. P-MT-27 vs P-MTg-43 and P-MT-34a vs P-MTg-42 respectively).

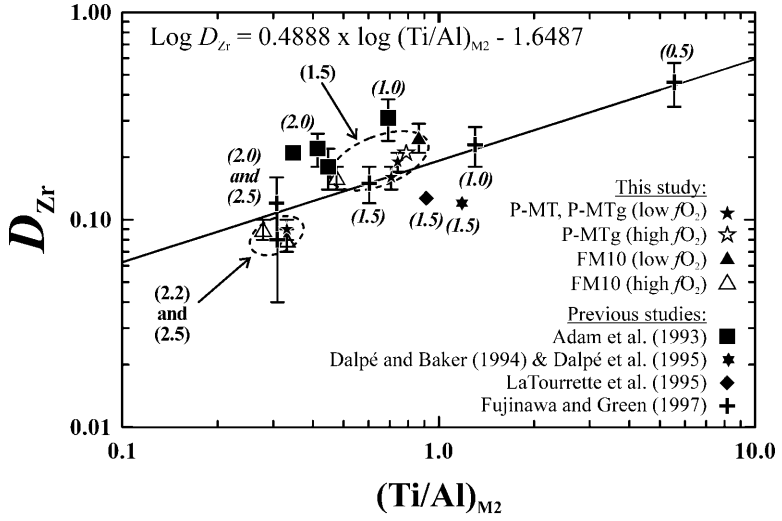

Fig. 4 Variation of D_{Zr} with the Ti/Al ratio in M2 octahedral site of amphibole run products as a function of pressure. Legend: P-MT-27, P-MTg-12, and P-MT-34a experiments at low oxygen fugacity [P-MT, P-MTg (low fO_2)]; P-MTg-43 and P-MTg-41 experiments at high oxygen fugacity [P-MTg (high fO_2)]; FM10-02 experiment at low oxygen fugacity [FM10 (low fO_2)]; FM10-23 and FM10-25 experiments at high oxygen fugacity [FM10 (high fO_2)]; run nos. 1388, 1389, 1393, 1395, and 1409 from Adam et al. (1993); run no. 3048T-1 from LaTourrette et al. (1995); run nos. 1702, 1705, 1666, 1664, and 1707 from Fujinawa and Green (1997); least-squares linear regression based on partition coefficients from this and previous experimental studies with the exception of runs 1388 and 1409 of Adam et al. (1993) (see text) (*filled line*). Numbers denote: run pressure in GPa (*italic numbers* refer to other experimental studies). Field denotes experiments from this study at 1.5 and 2.2–2.5 GPa

The effect of temperature on partition coefficient at fixed pressure and oxygen fugacity

We cannot observe an effect of temperature on partition coefficients because of the identical conditions used during experiments (e.g. P-MT-27 vs P-MTg-12). However, Adam and Green (1994) reported no variation in partition coefficients between an amphibole and basaltic melt within a range of 100 °C. We therefore believe that any temperature effect is small over the range of suitable magmatic temperatures for basalts where amphibole is stable.

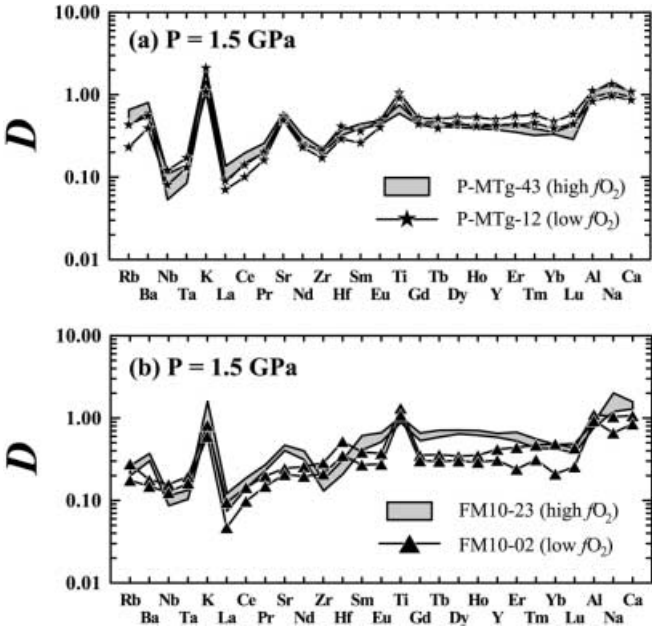

Fig. 5 The effect of oxygen fugacity on partition coefficients at different run pressures. **a** Experiments performed with the pargasitic material. **b** Experiments performed with the alkaline basalt material

Thermodynamic model applied to the amphibole/melt partitioning

The substitution of trace elements into crystallographic sites has been modeled using different thermodynamic relationships in order to explain and/or to predict partition coefficients (e.g. Beattie 1994; Blundy and Wood 1994). Based on partition coefficients these models can elucidate some physical and structural characteristics of the mineral without other detailed analytical techniques (e.g. van Westrenen et al. 1999). We will use the model described by Blundy and Wood (1994) because of its simplicity and its previous success in explaining the behavior of partition coefficients between amphibole and basaltic melt. The model can be used to extract physical properties of the mineral at different pressures, temperatures and compositions (Brenan et al. 1995; LaTourrette et al. 1995; Schmidt et al. 1996; Blundy 1997; Wood and Blundy 1997; van Westrenen et al. 1999; Wood et al. 1999).

Following Blundy and Wood (1994), the general equation can be written as:

$$D_i(P,T,X) = D_o(P,T,X) \times \exp \times \left[\frac{-4\pi\overline{E}N_A\left[\frac{r_o}{2}(r_i - r_o)^2 + \frac{1}{3}(r_i - r_o)^3\right]}{RT}\right] \quad (1)$$

where D_i (P,T,X) is the measured partition coefficient of a cation at the pressure, temperature and composition of interest, D_o (P,T,X) is the strain-free partition coefficient of the lattice-site for a series of isovalent cations at the same pressure, temperature and composition as D_i, $\overline{E}$ represents the Young's modulus of the lattice-site (in bar), N_A is the Avogadro's number (in mol^{-1}), r_o is the optimum ionic radius of the lattice-site (in nm; ionic radius from Shannon 1976), r_i is the ionic radius of the substitute cation (in nm), R is the gas constant (in J K^{-1} mol^{-1}) and T is the temperature (in kelvin).

Equation (1) can be used to fit the partition coefficients of an isovalent series of cations that occupy the same lattice-site (e.g. $REE^{3+} + Y^{3+}$ in the M4 site). By fitting a non-linear, least-squares regression to each isovalent cation series, D_o, r_o and $\overline{E}$ values can be extracted for each lattice site. Figure 6 shows a typical diagram where partition coefficients are plotted against the ionic radius for the P-MT-27 experiment. As shown in Fig. 6, it was possible to calculate D_o, $\overline{E}$ and r_o values for $(Ti, Hf, Zr)_{M2}$, $(Ta, Nb, Mg, Fe)_{M1}$, $(Fe, Ca, Sr)_{M4}$, $(REE, Y)_{M4}$ and $(Na, K, Rb)_A$ without constrained values. These results are listed in Table 5. This fitting procedure yields apparent values for r_o, $\overline{E}$ and D_o. For calcic amphiboles (i.e. tremolite and pargasite), the measured Young's modulus of the different lattice-sites are in general $\overline{E}_{M3} > \overline{E}_{M1} > \overline{E}_{M4} > \overline{E}_{M2} > \overline{E}_A$ (Comodi et al. 1991), whereas the calculated Young's moduli from partition coefficient values are in general $\overline{E}_{M1,3} > \overline{E}_{M2} > \overline{E}_{M4} > \overline{E}_A$ (for pargasite: Brenan et al. 1995; LaTourrette et al. 1995). The Young's modulus of a specific lattice site increases as the valency of the cation series increases as shown in Fig. 6 by the closing of the different near-parabolic curves between the $(Fe, Ca, Sr)^{2+}_{M4}$ and $(REE, Y)^{3+}_{M4}$ series (i.e. $\overline{E}_{M4}$ increases, Table 5). For the P-MT-27 experiment, the calculated and estimated Young's moduli are $\overline{E}_{M2} > \overline{E}_{M1} > \overline{E}_{M4} > \overline{E}_A$, which are closely related to the range of values reported by Brenan et al. (1995), LaTourrette et al. (1995) and to the $\overline{E}_{M4}$ value reported by Bottazzi et al. (1999). The calculated optimum ionic radius of the M4 site for P-MT-27 experiment does not correspond to the ionic radius of a major divalent element such as Ca, which occupies the same lattice site (ionic radius of $^{VIII}Ca = 0.112$ nm). Instead it corresponds to the ionic radius of Tb (i.e. ionic radius of $^{VIII}Tb = r_o = 0.104$ nm; Fig. 6). Similar observations were reported by Brenan et al. (1995), LaTourrette et al. (1995) and Bottazzi et al. (1999) for pargasites of similar composition to those in this study.

Variations of the amphibole lattice-site parameters as a function of the pressure and oxygen fugacity

Role of pressure

Figure 7 shows the variations in partition coefficients as a function of pressure for which a non-linear least-squares regression fit was obtained for each experiment using Eq. (1). Table 6 shows the results calculated for the different lattice-sites (M2, M4, A) where some D_{HFSE}, D_{REE} and D_{LILE} demonstrated variations greater than one standard deviation.

An increase in pressure affects at least three lattice-sites of the amphibole structure (Fig. 7 and Table 6). In general, the calculated Young's modulus decreases for the three lattice-sites with increasing pressure from 1.5 to 2.2 or 2.5 GPa. However, those $\overline{E}$ values are within or close to variations because of standard deviations of the partitioning data (Table 6). D_o also decreases as pressure increases (with the exception of the A site for FM10 experiments). Independently of D_o, the decrease in $\overline{E}$ for the majority of the different lattice sites with increasing pressure suggests that cations with radii far from r_o of a specific isovalent curve are relatively more affected by pressure than those closer to the optimum ionic radius. As for example D_{Rb}, which has ionic radius far from the r_o value for the A site, increases more rapidly than D_{Na} and D_K with increasing pressure, thus producing a lower calculated Young's modulus (the near-parabolic curve becomes wider) with increasing pressure (Fig. 7). This

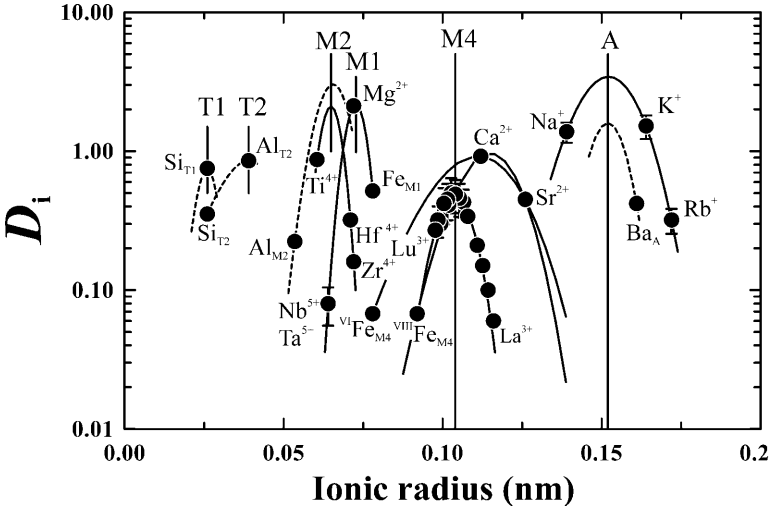

Fig. 6 Calculated least-squares regression lines obtained for partition coefficients of different groups of cations plotted against the ionic radius for P-MT-27 experiment. *Letters* denote tetrahedral sites ^{IV}(T1 and T2); octahedral sites ^{VI}(M1 and M2); distorted cubic site ^{VIII}M4; distorted cuboctahedron site ^{XII}A. *Lines* denote unconstrained non-linear least-squares regressions (*filled line*, see Table 5); constrained non-linear least-squares regressions (*dashed line*)

Table 5 Calculated and estimated lattice-site parameters for P-MT-27 experiment. Values in brackets represent qualitative results

Lattice-site	Charge	Coordination	Cation	D_o (GPa)	$\overline{E}$ (GPa)	r_o (nm)
A	1+	12	Na, K, Rb	3.44	110.43	0.152
	2+	12	Ba	[1.60[a]]	[315.552]	[0.152[b]]
M4	2+	8	Fe[c], Ca, Sr	0.97	153.121	0.115
		8	Fe[c, d], Ca, Sr	0.92	80.699	0.111
	3+	8	REE, Y	0.48	445.44	0.104
M1[e]	2+, 5+	6	Mg, Fe[f], (Nb, Ta)[g]	2.16	1985.12	0.073
M2	3+	6	Al[h]	[3.03[a]]	[937.84]	[0.065[i]]
	4+	6	Ti, Hf, Zr	2.10	2213.58	0.065
T2	4+, 3+	4	Si[j], Al[k]	[0.85[l]]	[520.01]	[0.039[m]]
T1	4+	4	Si[n]	[0.74[o]]	[5484.30]	[0.026[p]]

[a] Estimated value
[b] r_o was regressed from the 1+ cations of the A site
[c] D_{Fe} was calculated allowing 11.6% [0.070/(0.070 + 0.535) × 100] of the total ferrous-iron allocated to the M4
[d] Assuming six-fold coordination for Fe^{2+}
[e] M1 denotes the M1 and M3 sites combined (see text)
[f] D_{Fe} was calculated allowing 88.4% [0.535/(0.535 + 0.070) × 100] of the total ferrous-iron allocated to the M1 site
[g] Site occupancy following Foley et al. (1999)
[h] D_{Al} was calculated allowing 20.8% [0.550/(0.550 + 2.097) × 100] of the total aluminum allocated to the M2
[i] r_o was regressed from the 4+ cations of the M2 site.
[j] D_{Si} was calculated allowing 32.2% [(5.903−4.000)/5.903 × 100] of the total tetrahedral silicon allocated to the T2 site
[k] D_{Al} was calculated allowing 100% of the tetrahedral aluminum allocated to the T2 site
[l] D_o was assumed to be the calculated D_{Al} allocated for the T2 site.
[m] r_o was assumed to be the ionic radius of the ^{IV}Al.
[n] D_{Si} was calculated allowing 67.8% [(4.000/5.903) × 100] of the total tetrahedral silicon allocated to the T1 site
[o] D_o was assumed to be the calculated D_{Si} allocated for the T1 site.
[p] r_o was assumed to be the ionic radius of ^{IV}Si

behavior of D_{Rb} is particularly interesting because it has never been reported that increasing pressure increases partitioning of one set of elements that substitute into the large cavity of the A site (e.g. D_{Na}, D_K and D_{Rb}), whereas for other lattice sites partitioning decreases (e.g. D_{LREE} in the M4 and D_{HFSE} in the M2 lattice-sites) with increasing pressure for the same amphibole/basaltic melt pair. Pressure does not affect all D's equally even for those elements in the same lattice site. In such a case, the changes in pressure and the corresponding composition may create interesting trace element fractionations.

Based on compressibility experiments of a natural pargasite crystal, Comodi et al. (1991) observed a weak decrease in the different mean bond-lengths (e.g. ⟨A-O⟩, ⟨M4-O⟩ and ⟨M2-O⟩), which are indirectly related to the optimum ionic radius, with increasing pressure (0.0001 to 3.5 GPa). In these experiments it is difficult to generalize the effect of pressure on the size of the sites. However the r_o of the A and M2 lattice-sites are, in general, higher in amphiboles produced from P-MT and P-MTg compared with amphiboles synthesized from FM10, whereas the r_o of the M4 site is practically identical in both sets of amphiboles. These relative differences can be observed by the location of the fixed optimum ionic radii used from the P-MT-27 experiment (compare Fig. 7a–d). Such relative displacements of the optimum ionic radii in the FM10 experiments were caused by the relatively higher D_{Na} (smaller cation) compared with D_K and D_{Rb} (larger cations) in the A site and a higher D_{Ti} (smaller cation) compared with D_{Hf} and D_{Zr} (larger cations) in the M2 site as opposed to the P-MT and P-MTg experiments. The relationship between the optimum ionic radius and the mean bond-length suggests that amphiboles that crystallized from the FM10 material have lower ⟨A-O⟩ and ⟨M2-O⟩ mean bond-lengths than those crystallized from P-MTg material at an identical pressure (1.5 GPa) at high fO_2 (Fig. 7c, d). This is consistent with the higher proportion of large cations observed in the M2 and A sites, Ti_{M2} and K_A, for amphiboles crystallized in P-MTg-43 and P-MTg-41 compared with those crystallized in FM10-23 and FM10-25 experiments performed at identical or similar run conditions. However, variations in r_o are within errors calculated from partitioning and, in such a case, only detailed compressibility measurements may possibly answer these trends.

In summary, increasing pressure shows a similar behavior for HFSE and REE whereas the LILE behave in an opposite direction. Increasing pressure increases $D_{A\text{-site}}$ of the monovalent cations (or stays within one standard deviation) whereas $D_{M4\text{-site}}$ of trivalent cations and $D_{M2\text{-site}}$ of quadrivalent cations decrease (or stays within one standard deviation).

Role of oxygen fugacity

Figure 8 shows the variations in partition coefficients as a function of oxygen fugacity and Table 6 shows the results calculated for the different lattice sites at a fixed

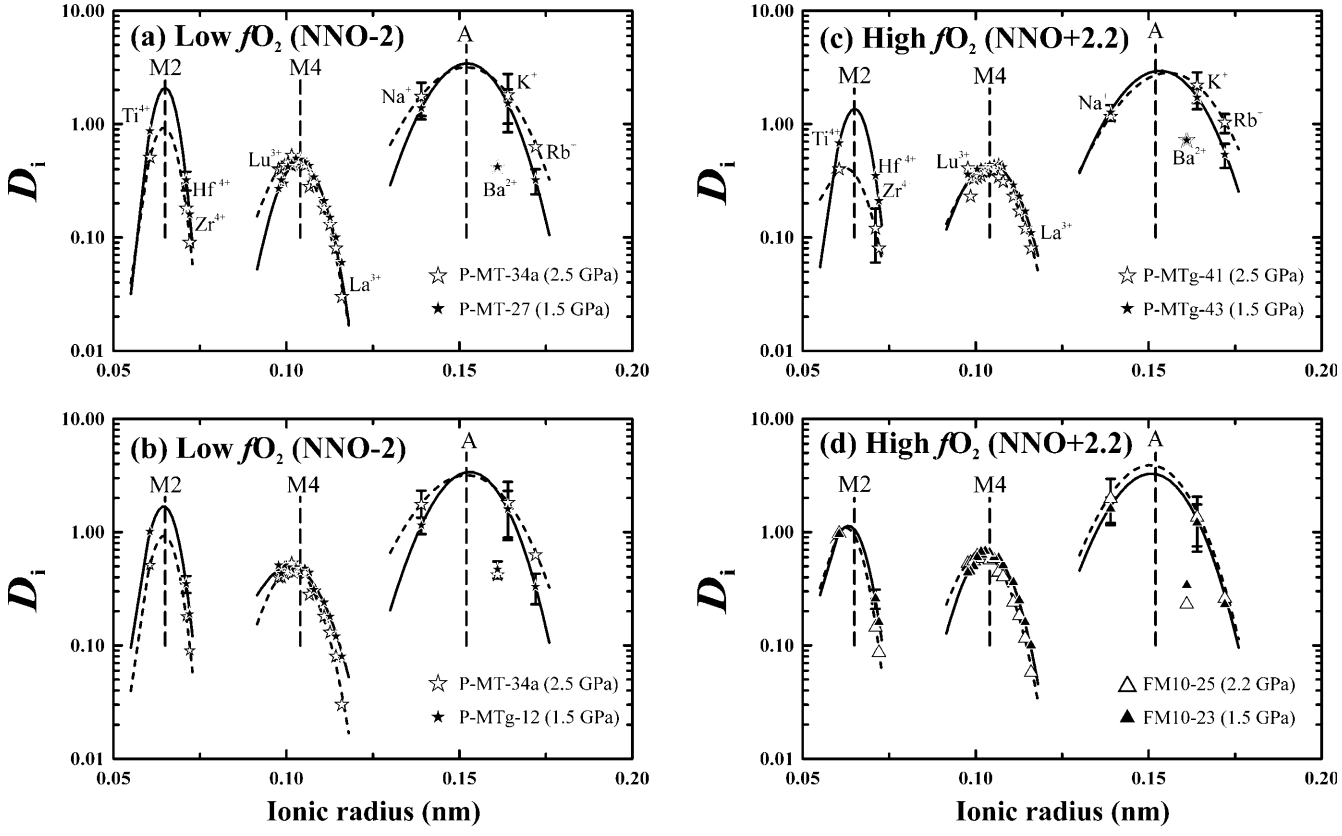

Fig. 7 Variations of partition coefficients as a function of ionic radius at different pressures. **a–c** Experiments performed with the pargasitic materials. **d** Experiments performed with the alkaline basalt material. *Lines* denote regression based on partition coefficients obtained for the low pressure experiments (*filled line*); regression based on partition coefficients obtained for the high pressure experiments (*dashed line*); r_o's regressed from P-MT-27 experiment for comparison in this and the subsequent figure (*vertical thick dashed line*; see Table 5)

pressure. A change in oxygen fugacity affects at least three lattice-sites in the amphibole structure, similar to the pressure effects (i.e. M2, M4 and A sites). The relatively large variations observed in partitioning at a fixed run pressure cannot be because of the variations in the run temperature but are mainly affected by the oxygen fugacity in the experiment. Increasing oxygen fugacity has a similar effect as increasing pressure on the lattice site parameters of the amphibole structure where both decrease D_o, $\overline{E}$ and r_o (Table 6). The greater relative change in D_K and D_{Rb} as opposed to D_{Na} for P-MT and P-MTg experiments resulted from a decrease in the Young's modulus ($\overline{E}$) for the A site with increasing fO_2. Such fO_2 variation also affects the optimum ionic radius of the A site where in general it increases. Relative shifts in r_o can be observed in the different P-MT and P-MTg experiments, especially for the P-MT-34a vs P-MTg-41 pair of experiments performed at high pressures (Fig. 8d). The variation in D_o as fO_2 increases is greater for the M2 site in general (~18 to 56% decrease) where variations in partition coefficients are more important than the two other lattice-sites (i.e. ~11 to 14% and ~6 to 19% decrease for A and M4 sites respectively). For the P-MT and P-MTg experiments, increasing the oxygen fugacity preferentially increases some D_{LREE}'s (e.g. D_{La}, D_{Ce}, D_{Pr}, D_{Nd}), compared with some D_{HREE}'s (e.g. D_{Tm}, D_{Yb}, D_{Lu}), which remain within one standard deviation. Such behavior has the effect of decreasing the calculated trivalent cation Young's modulus in the M4 site (i.e. $\overline{E}$ decreases; Fig. 8a, b, d). For FM10 experiments, we observed a peculiar behavior for the trivalent cations in the M4 site. Some D_{LREE}'s (i.e. D_{La}, D_{Ce}) and D_{HREE}'s (i.e. D_{Tm}, D_{Yb}, D_{Lu}) remained within one standard deviation whereas the other trivalent cations reached a maximum increase by a factor of ~2 as the oxygen fugacity increased (Fig. 8c and Table 6). In such a case, the Young's modulus shows an increase with increasing fO_2. Similar variations also affect the monovalent cations in the A site where D_{Na} and D_K increase more rapidly from NNO−2.0 to NNO + 2.2 as opposed to D_{Rb}, producing a higher $\overline{E}_A$ with increasing fO_2 (Fig. 8c).

Increasing the oxygen fugacity should directly affect the Fe^{3+}/Fe^{2+} ratio in the different run products. However, as mentioned above, the empirical model used to estimate the proportion of Fe^{3+} in one of our FM10 experiments (i.e. FM10-23) cannot confirm such a process because the proportion of Fe^{3+} in amphiboles produced at the high oxygen fugacity was found to be zero (Table 3). If the different cation proportions in the amphibole formulae remain identical as the oxygen fugacity increases, the oxidation of iron will result in a reduction of the mean bond-length (e.g. ⟨M1,2,3-O⟩)

Table 6 Calculated lattice-site parameters for experiments performed at different pressures and oxygen fugacities (unconstrained). D_o, maximum partition coefficient; $\overline{E}$, Young's modulus; r_o, optimum ionic radius

Starting material	Site[a]	D_o	$\overline{E}$ (GPa)	r_o[b] (nm)
P-MT-27[c]				
P-MT-34a	A	3.18 (1.64)	71.32 (22.4)	0.152 (0.001)
	M4	0.47 (0.05)	325.15 (16.2)	0.102
	M2	0.93 (0.41)	1711.53 (406.5)	0.065
P-MTg-12	A	3.40 (1.06)	117.01 (10.6)	0.153 (0.001)
	M4	0.50 (0.06)	207.56 (9.44)	0.101
	M2	1.68 (1.11)	1649.20 (684.8)	0.065 (0.001)
P-MTg-43	A	2.96 (0.34)	84.60 (9.3)	0.153
	M4	0.45 (0.02)	252.71 (53.07)	0.104
	M2	1.37 (0.20)	1601.47 (78.57)	0.065
P-MTg-41	A	2.84 (0.79)	66.47 (12.77)	0.156 (0.001)
	M4	0.38 (0.03)	243.09 (49.43)	0.103 (0.001)
	M2	0.49 (0.41)	1027.06 (805.37)	0.063 (0.002)
FM10-23	A	3.28 (1.26)	100.23 (15.20)	0.151 (0.001)
	M4	0.66 (0.06)	322.83 (13.47)	0.104
	M2	1.13 (0.26)	1012.56 (204.54)	0.063 (0.001)
FM10-25	A	3.90 (0.99)	97.11 (15.31)	0.150 (0.001)
	M4	0.64 (0.07)	284.2 (9.40)	0.102
	M2	1.10 (0.17)	1092.09 (144.21)	0.062 (0.001)
FM10-02	A	1.39 (0.21)	70.51 (8.59)	0.151 (0.001)
	M4	0.36 (0.08)	155.53 (91.47)	0.101 (0.003)
	M2	2.20 (0.53)	1658.64 (218.74)	0.065 (0.001)

[a] Calculated lattice-site parameters using D_{Na}, D_K, and D_{Rb} for the A site, D_{REE} (D_{La} up to D_{Lu}) and D_Y for the M4 site, and D_{Ti}, D_{Hf}, and D_{Zr} for the M2 site

[b] The optimum ionic radius that does not have parentheses imply the absence of significant calculated variations

[c] See Table 5. Values in parentheses represent the maximum variation calculated for each unconstrained lattice-site parameters using one standard deviation (i.e. $D+1\ \sigma$ and $D-1\ \sigma$) attached to each partition coefficient

where the relatively large Fe^{2+} (ionic radius = 0.078 nm) is oxidized to give a smaller cation (i.e. Fe^{3+}; ionic radius = 0.0645 nm).

In summary, increasing the oxygen fugacity affects partitioning differently from pressure where $D_{A\text{-site}}$ of monovalent and divalent cations and $D_{M4\text{-site}}$ of trivalent cations increase (or stay within one standard deviation) whereas $D_{M2\text{-site}}$ of quadrivalent cations decreases (or stay within one standard deviation). Variations of the optimum ionic radius (r_o) calculated for the A and M2 sites of the experimentally produced amphiboles suggest a change in major element composition (e.g. Ti_{M2}, K_A), reflecting variations in the bulk starting material. However, even if those variations are weak for the range of conditions and compositions used in this study, they are consistent with previous experimental studies investigating other silicate minerals (Blundy and Wood 1994).

Petrogenetic implications: the role of pressure and oxygen fugacity at upper mantle conditions

The observed variations in partition coefficients between amphibole and basaltic melt can be used to evaluate the role of amphibole in the petrogenetic evolution of an alkaline magmatic basaltic rock series potentially formed at different pressures and fO_2s.

Figure 9 shows the variation of Nb/Rb and Zr/Rb ratios vs Nb and Zr, respectively, for some basaltic lava flows of the Northern Canadian Cordillera. The most incompatible element enriched rocks (i.e. olivine–nephelinite and basanite) demonstrate a larger scatter in their Nb/Rb ratio and in their Zr/Rb ratio than the alkaline olivine basalts (Fig. 9).

Francis and Ludden (1995) suggested that nephelinite lava flows from the Northern Canadian Cordillera could result directly from the melting of amphibole in peridotite (i.e. amphibole-bearing lherzolite source). Based on our experiments performed with P-MT and P-MTg materials, we will demonstrate that the relatively large scatter observed in the Nb/Rb and Zr/Rb ratios for the olivine–nephelinites and basanites can be explained by partial melting of an amphibole-bearing lherzolite source at different pressures and oxygen fugacities. However, we have to keep in mind that the amphibole composition may also have an important contribution to those variations (e.g. Ti/Al). These P-MT and P-MTg partition coefficients were chosen instead of the alkaline basalt experiments because they were both performed at different pressures and oxygen fugacities analogous to the range of conditions observed in the upper mantle.

In our model, we used mineral proportions identical to Francis and Ludden's (1995) model with the exception of the amphibole (i.e. 14% instead of 10% in modal proportion) and garnet (i.e. 1% instead of 5% in modal proportion). These modifications were necessary because our peridotite composition was different from that of Francis and Ludden (1995) who did not include Rb, Nb and Zr in their modeled source. The initial amphibole-bearing lherzolite used in modeling was a natural sample taken from O'Reilly and Griffin (1988, sample: WGBM 16) for Rb (1.07 ppm), Nb (2 ppm) and Zr (12 ppm). This composition was chosen because no amphibole-bearing lherzolites have yet been found in the Canadian Cordillera (Francis and Ludden 1990, 1995; Shi et al. 1998). This amphibole-bearing lherzolite composition was normalized to contain 6 ppm Ce, which was the value used by Francis and Ludden (1995) for their modeled source. This was necessary to reproduce the more evolved basanites and alkaline olivine basalts from our starting composition. Tables 7, 8, 9 show the parameters used for the modeling the non-modal melting of an amphibole-bearing lherzolite by separating melts from their source followed by aggregating them together in a well-mixed reservoir [see Shaw 1970, Equ. (14)]. The modeled melting of the amphibole-bearing lherzolite occurred by two main processes as proposed by Francis and Ludden (1995). The first melting process involves the melting of amphibole to form clinopyroxene, garnet and melt (in wt fraction; Francis and Ludden 1995):

$$1.0\,\text{amph} \Rightarrow 0.1\,\text{cpx} + 0.3\,\text{gt} + 0.6\,\text{melt}$$

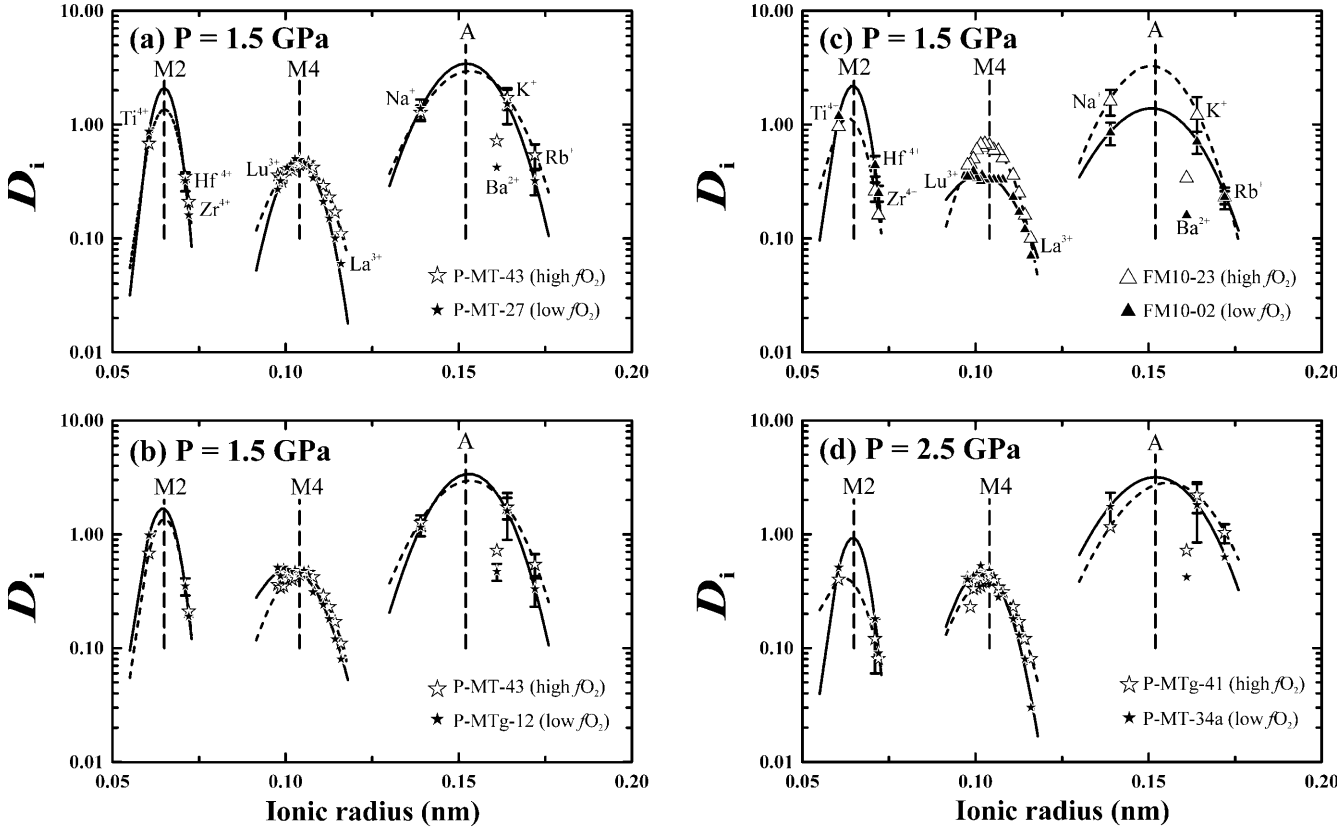

Fig. 8 Variations of partition coefficients as a function of ionic radius at different oxygen fugacities. **a**, **b, d** Experiments performed with the pargasitic materials. **c** Experiments performed with the alkaline basalt material. *Lines* denote regression based on partition coefficients obtained for the low oxygen fugacity experiments (*filled line*); regression based on partition coefficients obtained for the high oxygen fugacity experiments (*dashed line*)

After all the amphibole is consumed, which corresponds to ~6% of the total melting (i.e. f = fraction of melt produced = 0.06), the second melting process involves the reaction where clinopyroxene, orthopyroxene and garnet react to form olivine and melt (in wt fraction; Francis and Ludden 1995):

$$0.385\,\mathrm{cpx} + 0.385\,\mathrm{gt} + 0.23\,\mathrm{opx} \Rightarrow 0.23\,\mathrm{ol} + 0.77\,\mathrm{melt}$$

During the different melting processes, the D's for clinopyroxene, orthopyroxene, olivine and garnet were fixed while the D's for amphibole (i.e. D_{Rb}, D_{Nb} and D_{Zr}) were modified according to pressure and fO_2 conditions (Tables 7, 8, 9). There are no experimental studies showing the effect of pressure and oxygen fugacity on D_{Rb}, D_{Nb} and D_{Zr} for clinopyroxene, orthopyroxene, olivine and garnet.

The different models bracket the Nb/Rb and Zr/Rb ratios of olivine nephelinites and basanites from the Northern Canadian Cordillera (Fig. 9). A positive slope for the Nb/Rb and Zr/Rb ratios results from a higher $D_{\mathrm{Rb}}^{\mathrm{bulk}}$ compared with $D_{\mathrm{Nb}}^{\mathrm{bulk}}$ and $D_{\mathrm{Zr}}^{\mathrm{bulk}}$ because of the presence of amphibole (i.e. first process; Tables 7, 8, 9). The Nb/Rb and Zr/Rb ratios become horizontal or have a negative slope respectively, when amphibole has been totally melted (i.e. f = 0.06). This behavior results from a change of the bulk partition coefficient (i.e. D^{bulk}; see Tables 7, 8, 9).

The proposed models suggest that the variation of HFSE/Rb ratios observed in the most undersaturated alkaline basaltic lava flows of the Northern Canadian Cordillera may be caused by the melting of hydrous amphibole-bearing lherzolite at different pressures and oxygen fugacities. This scenario can be envisaged if the upper mantle was zoned with respect to oxygen fugacity by metasomatic fluids (e.g. Mattioli et al. 1989) during or before formation of Late Tertiary to Recent olivine nephelinite magmas beneath the Northern Canadian Cordillera. Based on coexisting ilmenite–spinel pairs from kimberlitic xenoliths, Haggerty and Tompkins (1983) have estimated different redox states of the lithosphere and asthenosphere depending upon the tectonic setting. They proposed that a fertile asthenosphere is relatively oxidized whereas depleted lithosphere is relatively reduced potentially resulting in a range of oxygen fugacities between the Iron–Wüstite (IW) and the FMQ buffers (Haggerty and Tompkins 1983). The range of oxygen fugacity suggested by Haggerty and Tompkins is similar to the range in our experiments. Shi et al. (1998) suggest that their bimodal xenolith suite (lherzolite and harzburgite) sampled from different localities along the Northern Canadian Cordillera represents lithospheric mantle that may have been

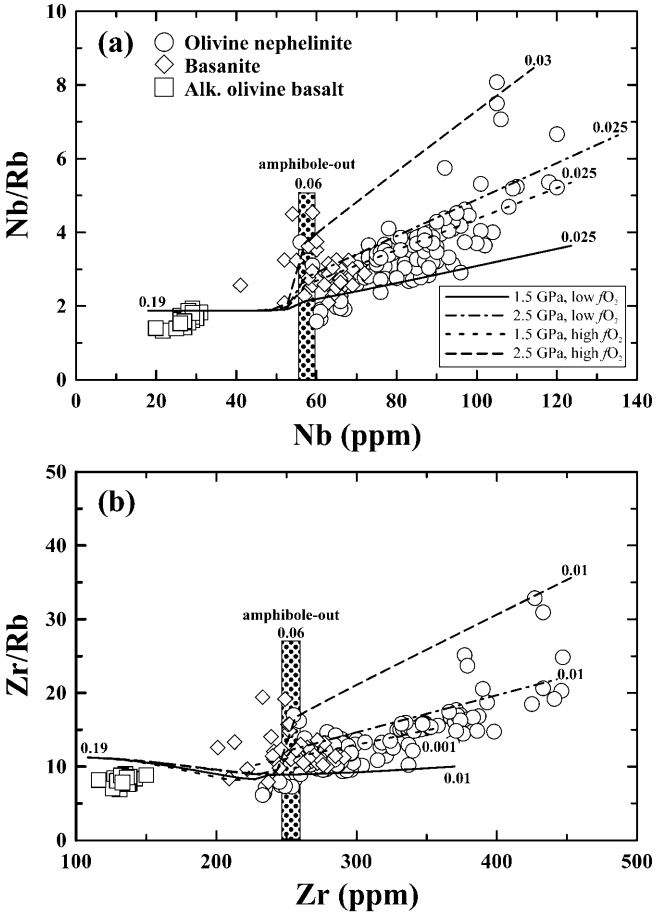

Fig. 9 Variation in incompatible elements within three alkaline lava suites located in the Northern Canadian Cordillera. **a** Nb/Rb ratio against Nb. **b** Zr/Rb against Zr. Data sources: Eiché et al. (1987), Francis and Ludden (1990, 1995), and Francis D. (personal communication). The different line patterns indicate non-modal melting of an amphibole-bearing lherzolite at both different pressures and oxygen fugacities. Abbreviations denote: model using P-MT-27 experiment (1.5 GPa, low fO_2); model using P-MT-34a experiment (2.5 GPa, low fO_2); model using P-MTg-43 experiment (1.5 GPa, high fO_2); model using P-MTg-41 experiment (2.5 GPa, high fO_2). Numbers indicate total fraction of melting (wt%). Note that the *amphibole-out* limit corresponds to approximately 6 wt% of melting (i.e. f = 0.06). See text for further discussion

influenced by an underlying hot asthenospheric mantle transporting volatiles. Such a process could, according to Haggerty and Tompkins (1983), influence the regional redox state of the lithosphere beneath the Northern Canadian Cordillera. Thus, when melted at differing fO_2 conditions and pressures the amphibole-bearing lherzolite could produce melts of significantly different trace element concentrations.

Studies of xenoliths support the presence of a range of redox conditions in the upper mantle below the Canadian Cordillera. Mattioli et al. (1989) estimated the redox state of various spinel-bearing lherzolite and harzburgite xenoliths sampled from various localities in the Northern Canadian Cordillera between ~0.5 log unit below FMQ to ~2.0 log unit above the FMQ for conditions between 900 and 1100 °C, 1.5 GPa. However, because of the absence of amphibole in xenoliths brought to the surface in the Northern Canadian Cordillera (Francis and Ludden 1990, 1995; Shi et al.

Table 8 Parameters used for the non-modal melting of an amphibole-bearing lherzolite. Mineral/melt partition coefficient from previous studies

	cpx[a]	opx[b]	ol[c]	gt[d]
Rb	0.02	0.0002	0.0002	0.007
Nb	0.01	0.0014	5.0E-5	0.004
Zr	0.22	0.0033	6.8E-4	0.5

[a] Values from Adam et al. (1993, run: 1389)
[b] Values from Kennedy et al. (1993, run: RPII 45) with the exception of D_{Rb} (best estimated value)
[c] Values from Kennedy et al. (1993, run: PO 49) with the exception of D_{Rb} (best estimated value)
[d] Values from Adam et al. (unpublished) [see Green (1994), and personal communication]

Table 9 Parameters used for the non-modal melting of an amphibole-bearing lherzolite. Bulk partition coefficient

	First process[a]				Second process[b]
	(1.5, low)	(2.5, low)	(1.5, high)	(2.5, high)	
Rb	0.047	0.090	0.078	0.148	0.003
Nb	0.013	0.007	0.013	0.005	0.002
Zr	0.050	0.041	0.057	0.039	0.057

[a] Where amphibole, clinopyroxene, orthopyroxene, olivine, and garnet are involved
[b] Where clinopyroxene, orthopyroxene, olivine, and garnet are involved (i.e. no amphibole). Note that garnet would be a metastable phase during the melting process at 1.5 GPa

Table 7 Parameters used for the non-modal melting of an amphibole-bearing lherzolite

Element	Amph-lh[a] (ppm)	Amph-lh[b] (ppm)	P-MT-27 (1.5, low)[c]	P-MT-34a (2.5, low)	P-MTg-43 (1.5, high)	P-MTg-41 (2.5, high)
Ce	3.5	6.0	(amph/melt partition coefficient from this study)			
Rb	1.07	1.83	0.32	0.63	0.54	1.04
Nb	2	3.43	0.08	0.04	0.08	0.03
Zr	12	20.6	0.16	0.09	0.21	0.08

[a] Amphibole-bearing lherzolite from O'Reilly and Griffin (1988, sample: WGBM 16) where the modal proportion of hydrous phase is <1% (amphibole and mica)
[b] Normalized to 6 ppm of Ce (see text)
[c] Number indicates run pressure (in GPa) and fO_2 (low ~NNO−2.0 and high ~NNO + 2.2)

1998) and the absence of quenched alkali-rich melts, it is difficult to prove this hypothesis. Our model does not conflict with the proposed model of Francis and Ludden (1995) regarding the presence or absence of amphibole in a metasomatized peridotite source, but it brings a new critical look at some of the scatter observed in the most undersaturated bulk rock analyses.

Acknowledgements We thank Steve R. Sutton for providing beam time on X26A at the National Synchrotron Light Source (NSLS, Brookhaven National Laboratory, NY) and for helping on data acquisition and data reduction. Mark Rivers, Saša Bajt and Patterson Nuessle are thanked for providing technical assistance with synchrotron X-ray-fluorescence microprobe. Gilles Gauthier and Amira Khoury are thanked for providing technical support on the LA-ICP-MS at the Université de Montréal (Quebec). We thank Hatten S. Yoder Jr. who graciously supplied the FM10 rock sample. C.D. personally thanks Don Francis for discussions on partition coefficients and modeling and for providing the use of his large data set on mafic volcanic rocks from the Northern Canadian Cordillera (some of which were unpublished). John Adam, Trevor H. Green and Soe H. Sie are thanked for exchanging unpublished data on garnet/basaltic melt partitioning. We thank John Adam, Tom LaTourrette and Timothy L. Grove for their constructive comments, which greatly improved the manuscript. This research was supported by NSERC and FCAR scholarships to C. Dalpé, NSERC grant OGP89662 and FCAR Nouveau Chercheur to D.R. Baker and DOE DE nos FG02-92ER14244, NASA NAG9-106, NSF EAR89-15699 grants to S.R. Sutton.

References

Adam J, Green TH (1994) The effects of pressure and temperature on the partitioning of Ti, Sr and REE between amphibole, clinopyroxene and basanitic melts. Chem Geol 117: 219–233

Adam J, Green TH, Sie SH (1993) Proton microprobe determined partitioning of Rb, Sr, Ba, Y, Zr, Nb and Ta between experimentally produced amphiboles and silicate melts with variable F content. Chem Geol 109: 29–49

Beattie P (1994) Systematics and energetics of trace-element partitioning between olivine and silicate melts: implication for the nature of mineral/melt partitioning. Chem Geol 117: 57–71

Blundy JD (1997) Experimental study of a Kiglapait marginal rock and implications for trace element partitioning in layered intrusions. Chem Geol 141: 73–92

Blundy JD, Wood BJ (1994) Prediction of crystal-melt partition coefficients from elastic moduli. Nature 372: 452–454

Bohlen SR (1984) Equilibria for precise pressure calibration and a frictionless furnace assembly for the piston-cylinder apparatus. Neues Jahrb Mineral Monatsh 9: 404–412

Bottazzi P, Tiepolo M, Vannucci R, Zanetti A, Brumm R, Foley SF, Oberti R (1999) Distinct site preferences for heavy and light REE in amphibole and the prediction of $^{Amph/L}D_{REE}$. Contrib Mineral Petrol 137: 36–45

Boyd FR, England JL (1960) Apparatus for phase-equilibrium measurements at pressures up to 50 kilobars and temperatures up to 1750 EC. J Geophys Res 65: 741–748

Brenan JM, Shaw HF, Ryerson FJ, Phinney DL (1995) Experimental determination of trace element partitioning between pargasitic amphibole and a synthetic hydrous andesitic melt. Earth Planet Sci Lett 135: 1–11

Brumm RC, Foley S, Tiepolo M, Vannucci R (1998) Trace element distribution between richteritic amphiboles and silicate melts, and contrasts to their behaviour in calcic amphiboles. Mineral Mag 62A: 250–251

Comodi P, Mellini M, Ungaretti L, Zanazzi PF (1991) Compressibility and high pressure structure refinement of tremolite, pargasite and glaucophane. Eur J Mineral 3: 485–499

Dalpé C (1998) Trace element partitioning between amphibole and basaltic melt. PhD Thesis, McGill University

Dalpé C, Baker DR (1994) Partition coefficient for rare-earth elements between calcic amphibole and Ti-rich basanitic glass at 1.5 GPa, 1100 EC. Mineral Mag 58A: 207–208

Dalpé C, Baker DR (1997) Evidence of pressure effects on LILE, HFSE and REE partitioning between calcic amphibole and basaltic liquid. Geol Assoc Can – Mineral Assoc Can 22: A-34 (Abstr)

Dalpé C, Baker DR, Sutton SR (1992) Partition coefficient of Ti, Cr, Ga, Rb, Sr, Y, Nb, and Zr between pargasite and nephelinic melt at 1.5 GPa. Eos (Trans Am Geophys Union) 73: 372 (Abstr)

Dalpé C, Baker DR, Sutton SR (1995) Synchrotron X-ray-fluorescence and laser-ablation ICP-MS microprobes: useful instruments for analysis of experimental run-products. Can Mineral 33: 481–498

Della Ventura G, Robert J-L (1990) Synthesis, XRD and FTIR studies of strontium richterites. Eur J Mineral 2: 171–175

Della Ventura G, Robert J-L, Bény J-M (1991) Tetrahedrally coordinated Ti^{4+} in synthetic Ti-rich potassic richterite: evidence from XRD, FITR, and Raman studies. Am Mineral 76: 1134–1140

Dunn T (1993) The piston-cylinder apparatus. In: Luth RW (ed) Short course handbook on experiments at high pressure and applications to the Earth's mantle. Mineral Assoc Can (Nepean) vol 21, pp 39–94

Eiché G, Francis D, Ludden J (1987) Primary alkaline magmas associated with Quaternary Alligator Lake volcanic complex, Yukon Territory, Canada. Contrib Mineral Petrol 95: 191–201

Foley S, Brumm RC, Tiepolo M, Bottazzi P, Oberti R, Vannucci R, Zanetti A (1999) HFSE site preferences and coupled/decoupled behavior of Ti, (Nb, Ta) and (Zr, Hf) in amphiboles. Eos (Trans Am Geophys Union) 80: S360 (Abstr)

Francis D, Ludden J (1990) The mantle source for olivine nephelinite, basanite, and alkaline olivine basalt at Fort Selkirk, Yukon, Canada. J Petrol 31: 371–400

Francis D, Ludden J (1995) The signature of amphibole in mafic alkaline lavas, a study in the Northern Canadian Cordillera. J Petrol 36: 1171–1191

Fujinawa A, Green TH (1997) Partitioning behaviour of Hf and Zr between amphibole, clinopyroxene, garnet and silicate melts at high pressure. Eur J Mineral 9: 379–391

Green TH (1994) Experimental studies of trace-element partitioning applicable to igneous petrogenesis – Sedona 16 years later. Chem Geol 117: 1–36

Green TH, Pearson NJ (1985) Experimental determination of REE partition coefficients between amphibole and basaltic to andesitic liquids at high pressure. Geochim Cosmochim Acta 49: 1465–1468

Haggerty SF, Tompkins LA (1983) Redox state of Earth's upper mantle from kimberlitic ilmenites. Nature 303: 295–300

Hawthorne FC (1983) The crystal chemistry of amphiboles. Can Mineral 21: 173–480

Hawthorne FC, Ungaretti L, Oberti R (1995) Site populations in minerals: terminology and representation of results of crystal-structure refinement. Can Mineral 33: 907–911

Hawthorne FC, Ventura GD, Robert J-L (1996) Short-range order of (Na, K) and Al in tremolite: an infrared study. Am Mineral 81: 782–784

Hudon P, Baker DR, Toft PB (1994) A high-temperature assembly for 1.91-cm (3/4-in.) piston-cylinder apparatus. Am Mineral 79: 145–147

Jenkins DM, Sherriff BL, Cramer J, Xu Z (1997) Al, Si, and Mg occupancies in tetrahedrally and octahedrally coordinated sites in synthetic aluminous tremolite. Am Mineral 82: 280–290

Jensen BB (1973) Patterns of trace element partitioning. Geochim Cosmochim Acta 37: 2227–2242

Kawamoto T, Hirose K (1994) Au–Pd sample containers for melting experiments on iron and water bearing systems. Eur J Mineral 6: 381–385

Kennedy AK, Lofgren GE, Wasserburg GJ (1993) An experimental study of trace element partitioning between olivine, orthopyroxene and melt in chondrules: equilibrium values and kinetic effects. Earth Planet Sci Lett 115: 177–195

Klein M, Stosch H-G, Seck HA (1997) Partitioning of high field-strength and rare-earth elements between amphibole and quartz-dioritic to tonalitic melts: an experimental study. Chem Geol 138: 257–271

Kress VC, Carmichael ISE (1991) The compressibility of silicate liquids containing Fe_2O_3 and the effect of composition, temperature, oxygen fugacity and pressure on their redox states. Contrib Mineral Petrol 108: 82–92

LaTourrette TZ, Hervig RL, Holloway JR (1995) Trace element partitioning between amphibole, phlogopite, and basanite melt. Earth Planet Sci Lett 135: 13–30

Leake BE, Woolley AR, Arps CES, Birch WD, Gilbert MC, Grice JD, Hawthorne FC, Kato A, Kisch HJ, Krivovichev VG, Linthout K, Laird J, Mandarino JA, Maresch WV, Nickel EH, Rock NMS, Schumacher JC, Smith DC, Stephenson NCN, Ungaretti L, Whittaker EJW, Youzhi G (1997) Nomenclature of amphiboles: report of the subcommittee on amphiboles of the international mineralogical association, commission on new minerals and mineral names. Can Mineral 35: 219–246

Liu C-Q, Masuda A, Shimizu H, Takahashi K, Xie G-H (1992) Evidence for pressure dependence of the peak position in the REE mineral/melt partition patterns of clinopyroxene. Geochim Cosmochim Acta 56: 1523–1530

Mattioli GS, Baker MB, Rutter MJ, Stolper EM (1989) Upper mantle oxygen fugacity and its relationship to metasomatism. J Geol 97: 521–536

Möller P (1988) The dependence of partition coefficients on differences of ionic volumes in crystal-melt systems. Contrib Mineral Petrol 99: 62–69

Nicholls IA, Harris KL (1980) Experimental rare earth element partition coefficients for garnet, clinopyroxene and amphibole coexisting with andesitic and basaltic liquids. Geochim Cosmochim Acta 44: 287–308

Oberti R, Vannucci R, Zanetti A, Tiepolo M, Brumm R (1998) On the correct determination of D_{Ti} in amph/liq and amph/cpx partitioning: the key role of the crystal-chemical mechanisms. Mineral Mag 62A: 1094–1095

O'Reilly SY, Griffin WL (1988) Mantle metasomatism beneath western Victoria, Australia: I. Metasomatic processes in Cr-diopside lherzolites. Geochim Cosmochim Acta 52: 433–447

Paris E, Mottana A, Della Ventura G, Robert J-L (1993) Titanium valence and coordination in synthetic richterite – Ti-richterite amphiboles. A synchrotron-radiation XAS study. Eur J Mineral 5: 455–464

Robert J-L, Della Ventura G, Raudsepp M, Hawthorne FC (1993) Rietveld structure refinement of synthetic strontium-rich potassium-richterites. Eur J Mineral 5: 199–206

Schmidt KH, Bottazzi P, Vannucci R, Mengel K, Foley SF (1996) Trace element partitioning between phlogopite and leucite–lamproite melt. In: VM Goldschmidt Conference, J Conf Abstr 1(1): 75

Schumacher JC (1997) Appendix 2. The estimation of the proportion of ferric iron in the electron-microprobe analysis of amphiboles. Can Mineral 35: 238–246

Shannon RD (1976) Revised effective ionic radii in oxides and fluorides. Acta Crystallogr, Sect A 32: 751–767

Shaw DM (1970) Trace element fractionation during anatexis. Geochim Cosmochim Acta 34: 237–243

Shi L, Francis D, Ludden J, Frederiksen A, Bostock M (1998) Xenolith evidence for lithospheric melting above anomalously hot mantle under the Northern Canadian Cordillera. Contrib Mineral Petrol 131: 39–53

Sweeney RJ, Green DH, Sie SH (1992) Trace and minor element partitioning between garnet and amphibole and carbonatitic melt. Earth Planet Sci Lett 113: 1–14

Tiepolo M, Vannucci R, Zanetti A, Brumm R, Foley SF, Bottazzi P, Oberti R (1998a) Partitioning of Nb and Zr between pargasite/kaersutite and melts in Ti-depleted systems. Mineral Mag 62A: 1519–1520

Tiepolo M, Vannucci R, Zanetti A, Brumm R, Foley SF, Bottazzi P, Oberti R (1998b) Fine-scale structural control of REE site-preference: the case of amphibole. Mineral Mag 62A: 1517–1518

Ulmer P (1989) The dependence of the Fe^{2+}–Mg cation-partitioning between olivine and basaltic liquid on pressure, temperature and composition, an experimental study to 30 kbars. Contrib Mineral Petrol 101: 261–273

van Westrenen W, Blundy JD, Wood BJ (1999) Crystal–chemical controls on trace element partitioning between garnet and anhydrous silicate melt. Am Mineral 84: 838–847

Ventura GD, Robert J-L, Hawthorne FC, Raudsepp M, Welch MD (1998) Contrasting patterns of $^{[6]}$Al order in synthetic pargasite and Co-substituted pargasite. Can Mineral 36: 1237–1244

Watson EB (1985) Henry's law behavior in simple systems and in magmas: criteria for discerning concentration-dependent partition coefficients in nature. Geochim Cosmochim Acta 49: 917–923

Wood BJ, Blundy JD (1997) A predictive model for rare earth element partitioning between clinopyroxene and anhydrous silicate melt. Contrib Mineral Petrol 129: 166–181

Wood BJ, Blundy JD, Robinson AC (1999) The role of clinopyroxene in generating U-disequilibrium during mantle melting. Geochim Cosmochim Acta 63: 1613–1620